Hemato-vascular specification requires *arnt1* and *arnt2* genes in zebrafish embryos

Authors: Hailey E. Edwards, Mary Jane Edgington, Jaclyn P. Souder, Daniel A. Gorelick

Center for Precision Environmental Health, Department of Molecular and Cellular Biology, Baylor College of Medicine, Houston, Texas, USA

Correspondence to DAG gorelick@bcm.edu

ABSTRACT

During embryonic development, a subset of cells in the mesoderm germ layer are specified as hemato-vascular progenitor cells, which then differentiate into endothelial cells and hematopoietic stem and progenitor cells. In zebrafish, the transcription factor *npas4l*, also known as *cloche*, is required for the specification of hemato-vascular progenitor cells. However, it is unclear if *npas4l* is the sole factor at the top of the hemato-vascular specification cascade. Here we show that *arnt1* and *arnt2* genes are required for hemato-vascular specification. We found that *arnt1;arnt2* double homozygous mutant zebrafish embryos (herein called *arnt1/2* mutants), but not *arnt1* or *arnt2* single mutants, lack blood cells and most vascular endothelial cells. *arnt1/2* mutants have reduced or absent expression of *etsrp* and *tal1*, the earliest known endothelial and hematopoietic transcription factor genes. *npas4l* and the *arnt* genes are PAS domain-containing bHLH transcription factors that function as dimers. We found that Npas4l binds both Arnt1 and Arnt2 proteins *in vitro*, consistent with the idea that PAS domain-containing bHLH transcription factors act in a multimeric complex to regulate gene expression. Our results demonstrate that *npas4l*, *arnt1* and *arnt2* act together to regulate endothelial and hematopoietic cell fate, where each gene is necessary, but by itself not sufficient, to drive hemato-vascular specification. Our results also demonstrate that *arnt1* and *arnt2* act redundantly in a transcriptional complex containing *npas4l*, but do not act redundantly when interacting with another PAS domain-containing bHLH transcription factor, the aryl hydrocarbon receptor. Altogether, our data enhance our

understanding of hemato-vascular specification and the function of PAS domain-containing bHLH transcription factors.

INTRODUCTION

Endothelial and hematopoietic cells are derived from a common mesodermal progenitor (Huber et al., 2004; Kataoka et al., 2011; Liao et al., 2000). In mice and zebrafish, fully multipotent hematopoietic stem cells (HSCs) are derived from specialized endothelial cells, called hemogenic endothelium (Hirschi, 2012; Kobayashi et al., 2014; Ramírez-Bergeron et al., 2004) The first hemato-vascular progenitors were traced back to the lateral plate mesoderm of zebrafish and in the extraembryonic yolk sac mesoderm of mice (Lee et al., 1994; Palis et al., 1999; Stainier et al., 1993). The complete mechanism of the specification of these hemato-vascular progenitors from the multipotent mesoderm remains elusive in mammals.

Many genes involved in embryonic hematopoiesis and vascular development are evolutionally conserved between zebrafish and mammals like mice and humans (Begley et al., 1989; Casie Chetty et al., 2017; Dooley et al., 2005; Ferrara et al., 1996; Herbert and Stainier, 2011; Kalev-Zylinska et al., 2002; Kataoka et al., 2011; Okuda et al., 1996; Wang et al., 1996). In zebrafish, the *neuronal PAS4-like* gene (*npas4l*), formerly known as *cloche,* is the earliest known transcription factor to drive the specification of hemato-vascular progenitors (Reischauer et al., 2016). *npas4l* mutants have a distinctive phenotype as they lack most endothelial and all hematopoietic cells (Stainier et al., 1995; Thompson et al., 1998).

Npas4l is a basic helix-loop-helix Per-Arnt-Sim (bHLH-PAS) transcription factor and is thought to be the master regulator of hemato-vascular specification (Reischauer et al., 2016). bHLH-PAS transcription factors are classified as Class I or Class II, which must dimerize to regulate gene transcription or repression (**Figure 1A**) (Card et al., 2005; Edwards and Gorelick, 2022; Pongratz et al., 1998). Npas4l is a Class I bHLH-PAS protein, but its Class II dimerization partner during hemato-vascular progenitor specification is not known. We hypothesized that Arnt1 or Arnt2 is the Class II

52 dimerization partner of Npas4l in zebrafish because *arnt1* and *arnt2* genes are expressed at the same
53 stages of embryo development as hemato-vascular specification (Baranasic et al., 2022; Prasch et al.,
54 2006; Reischauer et al., 2016; Tanguay et al., 2000).

55 To test this hypothesis, we examined hemato-vascular development in zebrafish with predicted
56 loss-of-function mutations in *arnt1* and *arnt2* genes. We find that Arnt1 and Arnt2 are essential for
57 hemato-vascular specification. Double homozygous *arnt1;arnt2* zebrafish embryos (herein called
58 *arnt1/2* mutants) phenocopy *npas4l* mutants and show lack of circulating blood, absence of
59 hematopoietic stem and progenitor cells, and dramatic reduction in the number of vascular endothelial
60 cells. We find that expression of *npas4l*-target genes requires *npas4l* and *arnt1* or *arnt2***.** Additionally,
61 we show that zebrafish Npas4l protein interacts with both zebrafish Arnt1 and zebrafish Arnt2 proteins
62 *in vitro*. Together, our results suggest that Arnt1 and Arnt2 act redundantly and form a transcriptional
63 complex with Npas4l that sits atop the hemato-vascular specification cascade.
64
65
66 **MATERIALS AND METHODS**
67
68 **Zebrafish**
69 Adult zebrafish were raised at 28.5°C on a 14-h light, 10-h dark cycle in the BCM Zebrafish Research
70 Facility in an Aquaneering recirculating water system (Aquaneering, Inc., San Diego, CA) and a
71 Tecniplast recirculating water system (Tecniplast USA, Inc., West Chester, PA). Wild-type zebrafish
72 were AB strain (Westerfield, 2000) and *arnt1* and *arnt2* mutant lines were generated on the AB strain.
73 Once the mutant lines were established, they were bred onto the *Tg(Fli1:EGFP)*^{y1} transgenic
74 background (Lawson and Weinstein, 2002). All procedures were performed in accordance with and
75 approved by the BCM Institutional Animal Care and Use Committee.
76
77 **Embryo collection**

78 Adult zebrafish were allowed to spawn naturally in pairs or in groups. Embryos were collected in
79 intervals of 20 minutes to ensure precise developmental timing or staged following collection, placed in
80 60 cm^2 Petri dishes at a density of no more than 100 per dish in E3B media (60X E3B: 17.2g NaCl,
81 0.76g KCl, 2.9g $CaCl_2$-$2H_2O$, 2.39g $MgSO_4$ dissolved in 1L Milli-Q water; diluted to 1X in 9L Milli-Q
82 water plus 100 µL 0.02% methylene blue), and then stored in an incubator at 28.5°C on a 14-h light,
83 10-h dark cycle.
84
85 **Genotyping adult zebrafish**
86 Genomic DNA was isolated from tail biopsies from individual adult zebrafish and incubated in 50 µL
87 ELB (10 mM Tris pH 8.3, 50 mM KCl, 0.3% Tween 20) with 0.5 µL proteinase K (800 U/ml, NEB) in 96
88 well plates, one sample per well, at 55°C for 8 hours. Proteinase K was inactivated by incubation at
89 98°C for 10 minutes and DNA was stored at -20°C. Genotyping was performed by PCR and high-
90 resolution melting curve analysis (HRMA) as described (Parant et al., 2009; Romano et al., 2017). All
91 melting curves were generated with a Bio-Rad CFX96 or CFX Opus 96 Real-Time System over a 70-
92 95°C range and analyzed with the Bio-Rad CFX Manager 3.1 or the Bio-Rad CFX Maestro 4.1
93 software. All mutations were confirmed by TA cloning and sequencing. All primers used for HRMA can
94 be found in **Table S1**.
95
96 **CRISPR-Cas9 Mutant Generation**
97 Cas9 mRNA and gRNAs for *arnt1* and *arnt2* mutants were generated as previously described (Romano
98 et al., 2017; Souder and Gorelick, 2019). Cas9 mRNA was transcribed from a linearized pT3TS-nCas9n
99 plasmid, Addgene #46757 (Jao et al., 2013). The target sequences were identified using CHOPCHOP
100 (Labun et al., 2016; Labun et al., 2019). Oligonucleotides were annealed to each other and cloned into
101 a pT7-gRNA plasmid, Addgene #46759 (Jao et al., 2013). Oligonucleotides utilized are shown in **Table**
102 **S1**. gRNAs were synthesized from plasmids using a MEGAshortscript T7 Transcription Kit (Invitrogen
103 AM1354) and purified.

104 One-cell-stage embryos were injected using glass needles pulled on a Sutter Instruments
105 Fleming/Brown Micropipette Puller, model P-97 and a regulated air-pressure micro-injector (Harvard
106 Apparatus, NY, PL1–90). Each embryo was injected with a 1nL solution containing one gRNA for *arnt1*
107 and one gRNA for *arnt2* (30 ng/μL per target), Cas9 mRNA (150 ng/μL), and 0.1% phenol red. Mixtures
108 were injected into the yolk of each embryo. Approximately 100 injected embryos per gRNA pair were
109 raised to adulthood and crossed to AB zebrafish to generate F1 embryos. F1 offspring with heritable
110 mutations were sequenced to identify mutations predicted to cause loss of function.
111
112 **Live Imaging**
113 Embryos were imaged with a Nikon SMZ25 microscope equipped with a Hamamatsu ORCA-Flash4.0
114 digital CMOS camera, or with a Nikon SMZ18 microscope equipped with a Nikon DS-Fi3 camera.
115 Images were equally adjusted for brightness and contrast in Adobe Photoshop CC 2020. Embryos and
116 larvae were anesthetized with 0.04% tricaine and imaged in Petri dishes containing E3B. All embryos
117 were genotyped after imaging.
118
119 **Whole-mount *in situ* hybridization (WISH)**
120 We used the following DNA plasmids to generate RNA probes: *egfl7, lmo2* (Sun et al., 2018), *etsrp* (gift
121 of Dr. Nathan Lawson, Addgene plasmid # 49005) (Moore et al., 2013), *tal1* (gift of Dr. Arne Lekven),
122 *npas4l* (gift of Dr. Leonard Zon) (Reischauer et al., 2016), *runx1* and *kdrl* (gifts of Dr. Mary Goll) (Li et
123 al., 2015). For *lmo2* and *egfl7,* RNA was extracted from 10 pooled 1 dpf wild-type embryos using TRIzol
124 Reagent (ThermoFisher Scientific, 15596026) and purified using RNA clean & concentration kit (Zymo
125 Research, R1019). cDNA was synthesized using iScript cDNA synthesis (BioRad, 1708890). *lmo2* and
126 *egfl7* were PCR amplified and Topo TA cloned into pCRII vector (Invitrogen, K4600-01). Primers used
127 to amplify *lmo2* and *egfl7* can be found in **Table S1**. All DNA clones were verified by sequencing.
128 Digoxigenin-labeled antisense RNA probes were synthesized using T7 or SP6. Colorimetric *in situ*
129 hybridization (ISH) was performed on fixed zebrafish embryos and larvae as previously described, with

130 5% dextran in the hybridization buffer (Lauter et al., 2011; Thisse and Thisse, 2008). Following ISH,
131 embryos were washed several times in 1x PBST (phosphate buffered saline, 0.01% Tween), cleared
132 with glycerol, or mounted in 3% methylcellulose on a class coverslip, and imaged on either a Nikon
133 SMZ18 stereoscopic microscope or an inverted Nikon ECLIPSE Ti2-E microscope. Embryos were then
134 genotyped. If embryos were older than 24 hpf, genomic DNA was extracted in 20 µL ELB (10 mM Tris
135 pH 8.3, 50 mM KCl, 0.3% Tween 20) with 0.2 µL proteinase K (800 U/ml, NEB) in 96 well plates, one
136 sample per well, at 55°C for 2 hours. If the embryos were 24 hpf or younger, they were first de-
137 crosslinked in 300 mM NaCl for 4 hours at 65°C and held at 4-8°C until DNA could be extracted.
138 Genomic DNA was extracted using the HotSHOT protocol (Dobrzycki et al., 2018). Briefly, embryos
139 were suspended in 10-20 µL of lysis buffer (50 mM NaOH) and incubated at 95°C for 30 minutes,
140 cooled to 4°C, then 1/10th the volume of neutralization buffer (1M Tris-HCl, pH 8.0) was added. Embryo
141 lysate was incubated at 4°C overnight before starting PCR reactions. DNA regions of interest were
142 amplified using one of two methods. The genes of interest were PCR amplified using JumpStart
143 REDTaq ReadyMix (Sigma-Milipore, P0982) according to the manufacturer's protocols. Alternatively,
144 the DNA regions of interest were PCR amplified in two successive reactions using HS Taq (Takara,
145 R007). The first PCR amplified a larger fragment of *arnt1* (about 700 bp) or *arnt2* (about 970 bp). Then
146 the product of the larger fragment was used as a template to amplify a smaller fragment of *arnt1* (about
147 400 bp) or *arnt2* (about 650 bp). After PCR amplification, the PCR products were sequenced to
148 determine the genotype. All primer sequences can be found in **Table S1.**
149
150 **Whole-mount *in situ* hybridization chain reaction (WIHCR)**
151 HCR Antisense RNA probe sets for *arnt1, arnt2,* and *npas4l,* HCR amplifiers, and HCR buffers were
152 obtained from Molecular Instruments, Inc (https://www.molecularinstruments.com/). Each gene had a
153 probe set size of 20. WIHCR was performed on fixed AB embryos between 4-6 somites, as previously
154 described (Choi et al., 2018; Ibarra-García-Padilla et al., 2021). Following HCR, embryos were washed
155 several times in 1x PBST and cleared in glycerol. All embryos were mounted in 75% glycerol and

156 imaged on a Nikon Ti2-E inverted microscope with Yokogawa CSU-W1 spinning disk confocal and
157 Photometrics Prime95b sCMOS camera.
158
159 **WIHCR Image Processing and Analysis**
160 All images used in processing and analysis were captured on the same day, using identical acquisition
161 controls. We selected only images where a clear, bilateral view of the presumptive lateral plate
162 mesoderm (LPM) and presumptive notochord was available (N=6 embryos from a single clutch, and
163 N=4 negative control embryos from the same clutch). Images of anterior and posterior views of the
164 embryos were collected. To calculate the number of 3D objects in a stack, we used Image J, FIJI
165 version 2.3.0/1.53q (Schindelin et al., 2012), and the 3D-OC plug-in (Bolte and Cordelières, 2006). A
166 custom threshold for each channel was applied to each image to filter out background autofluorescence
167 seen in the negative control embryos. The number of detected objects for probed samples was then
168 normalized to negative control by subtracting the average number of detected objects from control
169 embryos from the number of detected objects in probed embryos. We used ImageJ to calculate the
170 adjusted integrated intensity of probed and control embryos (Schindelin et al., 2012). First, maximum
171 intensity projections (MIP) of the z-stacks were created, then the region of interest (ROI) was drawn
172 around the areas with the highest concentration of *npas4l* expression (presumptive LPM) or around the
173 corresponding region of the presumptive LPM in the negative control embryos. The percent area of
174 pixels and the mean gray value for each channel were calculated and limited to the threshold. The
175 adjusted integrated density was then calculated by multiplying the percent area and the mean gray
176 value.
177
178 **O-dianisidine labeling of blood cells**
179 Zebrafish embryos were stained at approximately 72 hours post fertilization. Embryos were
180 dechorionated using 0.2% pronase in E3B media for 5-10 minutes and were gently triturated with a
181 1000µl pipette. Embryos were transferred to glass vials and submerged in o-dianisidine working

182 solution, prepared as described (Kafina and Paw, 2018). Vials were kept in the dark for 5 minutes
183 during staining. Samples were then fixed in 4% formaldehyde for 30 minutes at room temperature.
184 Embryos were washed in PBS-Tween 0.1% before mounting for imaging in 3% methylcellulose on a
185 glass dish or coverslip. Embryos were genotyped after imaging.
186
187 **Plasmid synthesis for microinjection and *in vitro* transfection**
188 Cloning of plasmids for expression in cultured cells was performed as follows. For npas4l-V5, we took
189 pCS2+npas4lORF (gift of Dr. Leonard Zon) that contains the open reading frame (ORF) of zebrafish
190 *npas4l* downstream of the CMV promoter. This plasmid was modified to include a C-terminal V5 tag
191 using Q5 Site-Directed Mutagenesis Kit (New England Biolabs, #E0554S). For arnt1-myc, we
192 commercially synthesized a plasmid containing CMV promoter driving a codon-optimized zebrafish
193 *arnt1* ORF (ENSDART00000081852.5) with a C-terminal myc tag (Twist Bioscience, San Francisco,
194 CA). For arnt2-myc, we commercially synthesized a gene block of the zebrafish *arnt2* ORF
195 (ENSDART00000158162.2, Integrated DNA Technologies). The gene block was integrated into a
196 plasmid containing a CMV promoter using pcDNA3.3-TOPO TA cloning kit (Invitrogen, K8300-01) in
197 accordance with manufacturer's instructions. A C-terminal HA tag was added using Q5 Site-Directed
198 Mutagenesis Kit (New England Biolabs, #E0554S). For microinjection, an SP6 promoter was inserted
199 upstream of the transcriptional start using Q5 Site-Directed Mutagenesis Kit (New England Biolabs,
200 #E0554S). All plasmids were confirmed by sequencing.
201
202 **Cell Culture and Transient Transfection**
203 HEK293T cells (gift from Dr. Charles Foulds), were thawed and maintained at 37°C in humidified 5%
204 CO_2 atmosphere incubator. Cells were cultured in DMEM supplemented with 10% fetal bovine serum
205 (FBS; Gibco, 2062564) and 1% penicillin-streptomycin (Gibco, 15140-122). After 24 hours of passaging
206 in a 100mm plate at a density of 2.2 x 10^6 cells per dish and reaching at least 70 confluency, the media
207 was changed to DMEM supplemented with 1% dialyzed FBS. Cells were transiently transfected with 12

208 µg of total DNA and Lipofectamine 2000 according to the manufacturer's instructions (Invitrogen,
209 2400439) with *npas4l-v5* together with either *arnt1-myc* or *arnt2-HA* plasmid DNA.
210
211 **Co-immunoprecipitation and Western blot**
212 Transiently transfected cells were washed with ice cold PBS and lysed in 500 µL of 1x RIPA buffer
213 containing Pierce Protease (ThermoScientific, A32955). Cells were sonicated in 6 x 30 second intervals
214 using a Bioruptor 300 Machine (Diagenode), then centrifuged for 10 minutes at 10,000g at 4°C. The
215 lysate (supernatant) was removed from the pellet and placed in fresh 1.5mL Eppendorf tube. Cell lysate
216 was precleared with Protein A beads (Invitrogen #159 18-014) for 30 minutes 4°C, incubated with either
217 5 µg of V5 antibody (ThermoFisher Scientific R960-25) or myc antibody (SantaCruz, SC-40) diluted
218 1:200 for 1 hour, then immunoprecipitated with 20 µL of Protein A beads for 1 hour at 4°C. The beads
219 were washed three times with RIPA buffer and once with PBS and finally suspended in 30µL of PBS.
220 Equal volume of 2x Laemmli Sample Buffer (BioRad, cat# 1610737) was added to each sample and
221 boiled for 5 minutes at 95°C then placed on ice. Samples were run on 4-20% Mini-PROTEAN TGX gels
222 (BioRad, cat# 4561093) and transferred onto PVDF membrane using Trans-Blot Turbo Transfer
223 System (BioRad) using the pre-defined Mixed MW program. The membranes were washed several
224 times with 1x Tris-Buffered Saline, 0.1% Tween 20 (TBST) (GBiosciences, R043) and incubated for 1
225 hour with agitation in 5% milk in 1x TBST. Membranes were probed with 1:1000 V5-HRP
226 (ThermoFisher Scientific, R960-25), 1:1000 myc-HRP (SantaCruz, SC-40), or 1:200 HA (Cell Signaling,
227 3724) antibodies rocking overnight at 4°C. Membranes were washed 5 times with 1xTBST on orbital
228 rocker for 15 minutes at room temperature. Membranes probed with the anti-HA antibody were then
229 probed with 1:10,000 IRDye 800CW donkey anti-rabbit (Licor, 926-32213) in 2.5%-5% milk in 1x TBST
230 for 1 hour and then washed multiple times with 1xTBST on orbital rocker for 5 minutes prior to imaging.
231 Membranes probed with HRP conjugated antibodies were developed using Clarity™ Western ECL
232 Substrate (BioRad, 170-5061). Membranes were imaged using BioRad ChemiDoc™ MP Imaging
233 System.

234

235 **Zebrafish embryo injection**

236 Embryo injections were performed as described (Westerfield, 2000) with the following modifications.
237 Plasmids containing either *npas4l, arnt1,* or *arnt2* were linearized by restriction enzyme digestion.
238 mRNA was transcribed using the mMessage mMachine kit (Invitrogen, AM1340) and purified with the
239 RNA clean & concentration kit (Zymo Research, R1019). Embryos were microinjected at the 1-cell
240 stage with 1 nL total volume containing either *npas4l* mRNA (50 pg mRNA) or a mixture of *arnt1* and
241 *arnt2* mRNA (50 pg each for 100 pg total mRNA). All solutions were injected into the yolk.

242

243 **TCDD exposure**

244 At 1-day post fertilization (dpf), embryos were exposed to 10 ng/mL 2,3,7,8-tetrachlorodibenzodioxin
245 (TCDD, AccuStandard Inc, D404N) or vehicle (0.1% DMSO). All treatments were performed on a single
246 clutch of at least 20 embryos. Embryos treated with vehicle were from the same clutches as embryos
247 treated with TCDD. Chemical exposures were performed on at least 2 clutches per genotype. Embryos
248 were raised at 28.5°C on a 14-h light, 10-h dark cycle until 3 dpf, when they were imaged and then
249 genotyped.

250

251 **Statistical Analysis**

252 All Statistical analyses were performed using Prism version 9.4.1 (GraphPad Software, Boston, MA).
253 Mendelian Frequencies Analysis: For the Chi-squared analysis of embryo and adult genotype ratios we
254 eliminated all 0 values from the analysis.
255 WISH Phenotype Frequency Analysis: For WISH images of *arnt1/2* mutants**,** we used a binomial test to
256 compare the observed distribution of embryos with the reduced expression phenotype to the calculated
257 expected number of *arnt1/2* mutants. Additionally, we performed a Spearman rank correlation analysis
258 on genotyped embryos to determine if there was a correlation between the number of mutant alleles
259 and the observed phenotype. Each genotype was assigned a number 0-4: with 0 indicating no mutant

260 alleles (wild-type siblings), 1 indicating one mutant allele (*arnt1* heterozygous and *arnt2* heterozygous
261 siblings), 2 indicating two mutant alleles (*arnt1* homozygous, *arnt2* homozygous, or *arnt1/2*
262 heterozygous siblings), 3 indicating three mutant alleles (*arnt1* homozygous; *arnt2* heterozygous and
263 *arnt1* heterozygous; *arnt2* homozygous siblings), and 4 indicating 4 mutant alleles (*arnt1/2* mutants).
264 The overserved phenotypes were assigned a number value: normal expression was coded as a 1 and
265 reduced expression was coded as 0.
266 WIHCR Image Analysis: For WIHCR image analysis, the variance was not assumed for *npas4l* and
267 *arnt2* samples. *arnt1* samples did not have a normal distribution, thus a non-parametric Mann-Whitney
268 test was performed. We were able to identify an outlier in the *arnt1* integrated intensity data using
269 Grubb's test (α=0.05), however, when this outlier was removed from analysis there was no change in
270 significance or Mann-Whitney U value.
271 TCDD Treatment Analysis: For TCDD treated embryos, unpaired Welch's *t*-tests were performed to
272 compare the average number of embryos with cardiotoxicity to the average number of embryos with a
273 normal phenotype from a given genotype.
274

275 **RESULTS**

276 ***arnt1/2* homozygous mutants lack circulating blood**

277 To determine if *arnt1* or *arnt2* is required for hemato-vascular development, we generated
278 heritable mutant alleles for *arnt1 (arnt1*^{bcm1} and *arnt1*^{bcm2}*)* and *arnt2 (arnt2*^{bcm3}*)* using CRISPR/Cas9. For
279 *arnt1*^{bcm1}*,* we generated zebrafish with a 5 bp insertion in exon 5, which results in a frameshift at amino
280 acid (AA) 126 and a premature stop codon in the first PAS domain at AA139. For *arnt1*^{bcm2}, we
281 generated zebrafish with an 11 bp deletion in exon 10, which results in a frameshift at AA230 and a
282 premature stop codon between the two PAS domains at AA250 (**Figure 1B**). We did not observe any
283 phenotypic differences between homozygous *arnt1*$^{bcm/bcm1}$ and *arnt1*$^{bcm2/bcm2}$ mutant embryos or larvae,
284 these fish will herein be called *arnt1* mutants. During embryogenesis and larval development, *arnt1*
285 mutants appear to have a normal phenotype and are indistinguishable from age-matched wild-type
286 larvae (**Figure 1D-E**). *arnt1* mutants are viable to adulthood and are fertile, consistent with previously
287 published *arnt1* mutants (Marchi et al., 2020). Maternal zygotic *arnt1* mutants did not show a
288 developmental phenotype and were indistinguishable from wild-type or zygotic *arnt1* mutants. For
289 *arnt2*^{bcm3}*,* we generated zebrafish with a 3 bp deletion and 1 bp insertion in exon 9, which resulted in a
290 missense mutation at AA286 and a premature stop codon between the two PAS domains at AA287
291 (**Figure 1C**). During embryogenesis and larval development, *arnt2*$^{bcm3/bcm3}$ embryos, herein called *arnt2*
292 mutants, were indistinguishable from wild-type embryos (**Figure 1D-F**). *arnt2* mutants were viable at 5
293 days post fertilization (dpf) but did not survive to adulthood, consistent with other independently
294 generated *arnt2* mutant zebrafish lines (Hill et al., 2009; Löhr et al., 2009).

295 Because Arnt1 and Arnt2 can interact with multiple Class I bHLH-PAS proteins (**Figure 1A**), we
296 examined if embryos that lacked both *arnt1* and *arnt2* had a hemato-vascular phenotype. To generate
297 these embryos, we crossed *arnt1*$^{bcm2/+}$*;arnt2*$^{bcm3/+}$ adult fish to each other. We observed all genotypes
298 at the expected Mendelian ratios in offspring at 24 to 48 hours post fertilization (**Table 1**). However,
299 *arnt1*$^{bcm2/bcm2}$*; arnt2*$^{bcm3/bcm3}$ embryos, herein called *arnt1/2* mutants, showed a clear phenotype (**Figure**
300 **1G**). These embryos lack all circulating blood (**Figure 1H-L, and Movies 3, 4, 7, 8**). All other

301 intermediate *arnt1;arnt2* genotypes, e.g., *arnt1*$^{bcm2/+}$*;arnt2*$^{bcm3/+}$, appeared phenotypically wild-type
302 (**Figure 1H, J, K, and Movies 1, 2, 5, 6**). These results suggest that *arnt1* and *arnt2* function
303 redundantly because only the *arnt1/2* double homozygous mutants show a phenotype. Additionally, the
304 *arnt1/2* mutant phenotype appears identical to the previously described *npas4l* mutant phenotype, also
305 known as *cloche* (Reischauer et al., 2016; Stainier et al., 1995). Like *npas4l* mutants, *arnt1/2* mutants
306 exhibit pericardial edema and have an enlarged heart atrium, likely a secondary effect of the lack of
307 blood and endocardial cells (**Figure 1G, Movies 3, 7**). Taken together, these data suggest that *arnt1*
308 and *arnt2* have a similar function as *npas4l*.
309 Next, we examined the frequencies of the genotypes in adult fish from *arnt1*$^{bcm2/+}$*; arnt2*$^{bcm3/+}$
310 parents. Given that *arnt2* mutants are not viable as adults, these adults can be one of six possible
311 genotypes. Interestingly, we did not observe the expected Mendelian ratios of alleles in these adult fish
312 (**Table 2**; X^2(df=5, N=138) = 45.57, p<0.0001, N=138 offspring from two different clutches). There is a
313 reduction in the number of observed *arnt1*$^{bcm2/bcm2}$;*arnt2*$^{bcm3/+}$ heterozygous adults compared to the
314 expected number. We hypothesize that the number of *arnt1* and *arnt2* wild-type alleles correlates with
315 the likelihood of juvenile fish surviving to adulthood.
316
317 ***arnt1/2* mutants have reduced expression of hematopoietic and endothelial cells**
318 We hypothesized that the Arnt proteins are dimerization partners with Npas4l and that *arnt1/2*
319 mutants would exhibit the same phenotypes as *npas4l* mutants. Therefore, we examined *arnt1/2*
320 mutant embryos for additional phenotypes found in *npas4l* mutants. Previous studies determined that
321 *npas4l* mutants lack almost all endothelial cells, except a population of endothelial cells located in the
322 lower trunk and caudal tail of the larvae (Liao et al., 1997; Reischauer et al., 2016; Stainier et al., 1995).
323 To determine if our *arnt1/2* mutants showed a similar reduction in endothelial cells, we performed
324 whole-mount *in situ* hybridization (WISH) on 2 dpf embryos for *kdrl* (*flk-1)*. *kdrl*, a widely used marker of
325 endothelial cells in blood vessels, is essential for the development of blood vessels in mice and

326 zebrafish (Dumont et al., 1995; Liao et al., 1997; Shalaby et al., 1997). We found that *arnt1* mutants,
327 *arnt2* mutants, and wild-type embryos showed clear expression of *kdrl* in blood vessels at 2 dpf (**Figure**
328 **2A-C**, N=2-5 biological replicates per genotype per probe, 10-100 embryos examined per biological
329 replicate). In contrast, *arnt1/2* mutants had a reduced number of *kdrl*-positive cells at 2 dpf (**Figure 2D**).
330 The *kdrl*-positive cells present in the *arnt1/2* mutant were in the caudal tail and likely comprised a
331 portion of the caudal vein (**Figure 2D'**). To determine if this population of cells was present earlier in
332 development we bred *arnt1*$^{bcm2/+}$*; arnt2*$^{bcm3/+}$ onto a Tg(*fli1:egfp*^{y1}*)* transgenic background, which labels
333 all blood vessels and the pharyngeal arches of the developing embryos. At 1 dpf, *arnt1* mutants, *arnt2*
334 mutants, and wild-type embryos had GPF-positive vasculature structures (**Figure 2I-K,** N=2 biological
335 replicates, with 21-131 embryos per clutch, 232 embryos total). Within the tails of these embryos the
336 dorsal aorta, caudal vein, and intersegmental vessels are clear and present (**Figure 2I'-K'**). In contrast,
337 *arnt1/2* mutants had reduced GFP-positive vascular structures (**Figure 2L).** Within these embryos, only
338 the extreme caudal vein was fluorescent (**Figure 2L'**). This population of endothelial cells is also seen
339 in *npas4l* mutants (Liao et al., 1997). Together these results suggest that *arnt1* or *arnt2* is required for
340 *npas4l*-dependent blood vessel development.

341 In addition to a clear reduction of endothelial cells, *npas4l* mutants show a reduction in the
342 number of hematopoietic stem cells (HSC) (Stainier et al., 1995; Thompson et al., 1998). To determine
343 if *arnt1/2* mutants contain HSCs, we examined *runx1* expression by WISH. *runx1* is a marker of HSCs
344 and is required for definitive hematopoiesis in zebrafish (Kalev-Zylinska et al., 2002). At 48 hpf, *runx1*-
345 positive HSCs are known to localize to the area between the dorsal aorta and the posterior caudal vein
346 (Lam et al., 2009; North et al., 2009). At 2 dpf, *arnt1* mutants, *arnt2* mutants, and wild-type embryos all
347 contain *runx1*-positive cells near the dorsal aorta (**Figure 2E-G**). However, *arnt1/2* mutants have little or
348 no *runx1* labeling in this region (**Figure 2H**). This suggests that *arnt1* or *arnt2* is necessary for
349 hematopoietic cell development during embryogenesis, just like *npas4l* (Liao et al., 1997; Liao et al.,
350 1998; Stainier et al., 1995; Thompson et al., 1998).

351

352 **Hematopoietic and endothelial progenitor populations are reduced in *arnt1/2* mutants**

353 Hemato-vascular progenitor specification from the multipotent mesoderm begins in mid-
354 gastrula, around shield stage, and peaks during segmentation (Vogeli et al., 2006). Npas4l is thought to
355 directly upregulate target genes that cause cells to differentiate into endothelial cells and hematopoietic
356 stem and progenitor cells. If Npas4l, Arnt1 and Arnt2 act in tandem to regulate target gene expression,
357 then we expect that Npas4l-target genes would be downregulated in *arnt1/*2 mutants. Therefore, we
358 hypothesized that Npas4l-target genes would be downregulated in *arnt1/*2 mutants. We focused on
359 four putative *npas4l* target genes known to be important for the hemato-vascular lineage: *etsrp (etv2),*
360 *tal1, lmo2 (scl),* and *egfl7* (Marass et al., 2019; Sumanas and Lin, 2006; Sumanas et al., 2005). We bred
361 *arnt1*$^{bcm2/+}$*; arnt2*$^{bcm3/+}$ adults to each other to generate embryos that were *arnt1/2* mutant, *arnt1* mutant,
362 *arnt2* mutant, wild-type, and all other intermediate genotypes (referred to as *arnt1/2* siblings). At the 2-6
363 somite stages (about 10-14 hpf), *npas4l* mutant embryos show a reduction of expression in *etsrp*, *tal1,*
364 and *lmo2* (Reischauer et al., 2016; Thompson et al., 1998). We examined the expression of these
365 genes in *arnt1/2* mutants and *arnt1/2* siblings between 4-6 somite stage (**Figure 3**). We found that 7%
366 of embryos from *arnt1*$^{bcm2/+}$*;arnt2*$^{bcm3/+}$ parents showed reduced expression of *etsrp* compared to
367 siblings, (**Figure 3A-B**, *N*=4 biological replicates, 80-250 embryos per clutch, 604 embryos total). This
368 did not differ from the expected Mendelian ratio of *arnt1/2* mutants (6.25%; binomial test, $p>0.05$). To
369 confirm that these embryos were in fact *arnt1/2* mutants, following WISH we genotyped 24 embryos
370 with reduced expression of *etsrp* and found that 100% were *arnt1/2* mutants. We also genotyped 26
371 embryos with normal expression of *etsrp,* only two of which were *arnt1/2* mutants (**Table S2**). To
372 examine if there is an association between the number of mutant alleles and the observed phenotype,
373 we performed a Spearman Rank correlation test (see Methods for details) and found that there is a
374 statistically significant correlation between the number of mutant alleles and the observed phenotype
375 (*Spearman correlation,* r= -0.9, $p<0.001$). We conclude that the expression of *etsrp* is reduced in
376 *arnt1/2* mutants compared to wild-type.

377 We found that 7% of embryos from arnt*1*$^{bcm2/+}$*; arnt2*$^{bcm3/+}$ parents showed reduced expression of
378 *tal1* compared to *arnt1/2* siblings (**Figure 3C-D,** N=6 biological replicates, 60-300 embryos per clutch,
379 681 embryos total). This did not differ significantly from the expected Mendelian ratio of *arnt1/2* mutants
380 (binomial test, p>0.05). To confirm these embryos were in fact *arnt1/2* mutants, we genotyped 18
381 embryos with reduced expression and confirmed that 83% (15 of 18 embryos) of these embryos were
382 *arnt1/2* mutants (**Table S3**). We genotyped 11 embryos with normal expression of *tal1,* none of which
383 were *arnt1/2* mutants (**Table S3**). To examine if there is a relationship between the number of mutant
384 alleles and the observed phenotype, we performed a Spearman Rank correlation test and found that
385 there is a statistically significant correlation between the number of mutant alleles and the observed
386 phenotype (*Spearman correlation,* r= -0.6, p<0.005). We conclude that the expression of *tal1* is reduced
387 in *arnt1/2* mutants compared to wild-type.
388 We found that 11% of embryos from *arnt1*$^{bcm2/+}$*;arnt2*$^{bcm3/+}$ parents showed reduced expression
389 of *lmo2* compared to siblings (**Figure 3D-E,** N=2 biological replicates, 95-175 embryos per clutch, 270
390 embryos total). This did significantly differ from the expected 6.25% Mendelian ratio of *arnt1/2* mutants
391 (binomial test, p<0.01). To test for a phenotype-genotype correlation, we genotyped 185 embryos
392 following labeling for *lmo2:* 160 embryos with normal *lmo2* expression and 25 embryos with reduced
393 *lmo2* expression. Of the 25 embryos with reduced expression of *lmo2*, we observed 8 embryos that
394 were *arnt1/2* mutants, 8 embryos with three mutant alleles, 4 embryos with two mutant alleles, 3
395 embryos with one mutant allele, and 2 wild-type embryos (**Table S4**). Of the 160 embryos with normal
396 expression of *lmo2*, 5 embryos were *arnt1/2* mutants, 36 embryos had three mutant alleles, 64 embryos
397 had two mutant alleles, 46 embryos had one mutant allele, and 9 were wild-type embryos (**Table S4**).
398 To examine if there is a relationship between the number of mutant alleles and the observed
399 phenotype, we performed a Spearman rank correlation and found that there is a statistically significant
400 correlation between the number of mutant alleles and the observed phenotype (*Spearman correlation*, r
401 = -0.2, p<0.01). We conclude that the expression of *lmo2* is reduced in *arnt1/2* mutants compared to
402 wild-type.

403 We examined the expression of *egfl7* at 10-somite stage embryos from *arnt1*$^{bcm2/+}$*; arnt2*$^{bcm3/+}$
404 parents. We observed *egfl7* expression in portions of the ALPM and PLPM in wild-type and in 95% of
405 the embryos from *arnt1*$^{bcm2/+}$*; arnt2*$^{bcm3/+}$ parents, but no expression of *egfl7* in the anterior of 5% of
406 embryos from *arnt1*$^{bcm2/+}$*; arnt2*$^{bcm3/+}$ parents, N=11 of 214 embryos (**Figure S1,** N=2 biological
407 replicates, 94-120 embryos per clutch, 214 total embryos, and age-matched wild-type embryos, N=1
408 biological replicate, 28 embryos). This did not differ from the expected Mendelian ratio of *arnt1/2*
409 mutants (6.25%; binomial test, p>0.05). To examine if there is a relationship between the number of
410 mutant alleles and the observed phenotype, we performed a Spearman Rank correlation test and found
411 that there is a statistically significant correlation between the number of mutant alleles and the observed
412 phenotype (*Spearman correlation,* r= -0.5, p<0.001) (**Table S5**). We conclude that the expression of
413 *egfl7* is reduced in *arnt1/2* mutants compared to wild-type.
414 These results support the idea that *npas4l*, *arnt1* and *arnt2* regulate identical target genes for
415 hemato-vascular specification. *arnt1* and *arnt2* could interact with *npas4l* at the same level of the
416 pathway, consistent with bHLH-PAS transcription factors acting as heterodimers. Alternatively, it is
417 possible that *arnt1* and *arnt2* act upstream of *npas4l*. To distinguish among these ideas, we tested
418 whether *npas4l* expression was reduced in *arnt1/2* mutants. At the 2-4 somite stage, *arnt1/2* mutants
419 exhibit normal expression of *npas4l* in the lateral plate mesoderm, indistinguishable from age-matched
420 wild-type embryos (**Figure S2, Table S6,** N=2 biological replicates, 68-100 embryos per clutch, 168
421 total embryos). This result indicates that *npas4l* expression occurs independently of *arnt1* and *arnt2*.
422 We conclude that *npas4l* does not act downstream of *arnt1* or *arnt2*. Taken together, our results
423 suggest that *arnt1* and *arnt2* act in conjunction with *npas4l* during hemato-vascular specification.
424

425 ***arnt1* and *arnt2* expression is ubiquitous and colocalizes with *npas4l* expression**

426 If *arnt1, arnt2* and *npas4l* act together to specify hemato-vascular progenitor cells, then all three
427 genes should be expressed in the same cells in the lateral plate mesoderm. To determine if *arnt1,*

428 *arnt2,* and *npas4l* are expressed in the same cells, we performed whole-mount *in situ* hybridization
429 chain reaction (WIHCR) on wild-type zebrafish embryos at the 4-somite stage (approximately 10.5 hpf).
430 At this stage, *npas4l* is robustly expressed in the LPM (Reischauer et al., 2016). We found that *arnt1*
431 and *arnt2* are expressed ubiquitously throughout the embryo at this stage, although both genes appear
432 to be expressed at low levels (**Figure 4A and Figure S3A**, N=3 biological replicates, 5-9 embryos per
433 replicate, 22 embryos total).

434 Because no previous publications examined the spatial distribution of *arnt1* or *arnt2* mRNA in
435 embryos younger than 24 hpf (Löhr et al., 2009), we tested whether background or autofluorescence
436 influenced our results. Samples probed for *arnt1*, *arnt2,* and *npas4l* were compared to negative control
437 embryos, embryos from the same clutch that underwent the same WIHCR protocol, but in the absence
438 of anti-sense RNA probe sets (**Figure 4B and Figure S3B**, N=3 biological replicates, 6-12 embryos per
439 replicate, 28 embryos total)***.*** We verified that the observed *npas4l*, *arnt1,* and *arnt2* expression was
440 specific using two different image analysis tools. First, we analyzed representative images in 3-
441 dimensions using the ImageJ plug-in "3D Count Objects" (Bolte and Cordelières, 2006). The number of
442 objects above a set threshold was measured for each channel and then normalized to background by
443 subtracting the average number of objects detected in the corresponding channel of the negative
444 control embryos. *npas4l-, arnt1-*, and *arnt2*-positive objects were all detected in the posterior of the
445 embryos (**Figure 4C-E**). Second, we analyzed the expression of *arnt1* and *arnt2* in the presumptive
446 LPM by drawing regions of interest (ROIs) encompassing the observed *npas4l* signal*,* and then
447 measured the percent area of expression and the mean gray intensity above the threshold for each
448 channel. The integrated intensity was calculated by multiplying the percent area by the mean grey
449 intensity, thus taking both brightness and area of signal into consideration (**Figure 4F-H, Figure S3 C-**
450 **E**). We found that *npas4l, arnt1,* and *arnt2* all showed statistically significantly more expression in
451 experimental embryos compared to the negative control, as measured by both number of objects and
452 integrated intensity of objects in the LPM (**Figure 4F-H,** *npas4l* Welsh's t-test, $p<0.0001$; *arnt2* Welsh's
453 t-test, $p<0.0001$; *arnt1* Mann-Whitney test, $p<0.0001$).

454 We asked whether the expression of *npas4l*, *arnt1* and *arnt2* was the same in the anterior LPM
455 (ALPM) and posterior LPM (PLPM). *npas4l* and its associated downstream targets exhibit more
456 expression in the PLPM compared to the ALPM in embryos throughout segmentation (Liao et al., 1997;
457 Liao et al., 2000; Marass et al., 2019; Mattonet et al., 2022; Qian et al., 2005; Stainier et al., 1995). At 4-
458 6 somite stage embryos, we found that expression of *npas4l* and *arnt2* was greater in the PLPM than in
459 the ALPM, but the expression of *arnt1* was similar in both regions (**Figure S3C, S3E,** *npas4l* Welsh's t-
460 test, $p<0.0001$; *arnt2* Welsh's t-test, $p<0.005$). We conclude that *arnt1* and *arnt2* are expressed within
461 the *npas4l*-positive LPM, consistent with our hypothesis that all 3 genes together regulate the
462 specification of hemato-vascular progenitor cells.
463

464 **Expression of *npas4l*-target genes requires *npas4l*, *arnt1* and *arnt2***

465 *npas4l* is not expressed until tailbud stage (Reischauer et al., 2016). A previous study
466 demonstrated that ectopic expression of *npas4l* in shield-stage embryos, prior to the onset of
467 expression of endogenous *npas4l*, resulted in upregulation of and ectopic expression of early hemato-
468 vascular genes *etsrp* and *tal1* (Reischauer et al., 2016). We suspect that upregulation of *npas4l* target
469 genes occurred because *arnt1* and *arnt2* are ubiquitously expressed at shield stage. Single cell RNA
470 sequencing studies detected *arnt1* and *arnt2* mRNA throughout gastrulation, which encompasses
471 shield stage, in zebrafish embryos (Baranasic et al., 2022). To test whether expression of *npas4l*-target
472 genes requires *npas4l*, *arnt1,* and *arnt2*, we injected wild-type embryos at the 1-cell stage with either
473 *npas4l* mRNA or *arnt1* and *arnt2* mRNA. The embryos were fixed at shield stage, and assayed for
474 expression of *tal1* or *lmo2* using WISH. Wild-type embryos injected with *npas4l* mRNA exhibited robust
475 expression of *tal1* compared to uninjected control embryos (**Figure 5A-B**). In contrast, embryos
476 injected with *arnt1* and *arnt2* mRNA showed little or no expression of *tal1*, similar to uninjected embryos
477 (**Figure 5C**). This suggests that neither *arnt1* nor *arnt2* can drive expression of *tal1* in the absence of
478 *npas4l*. To directly test whether *arnt1* and *arnt2* can drive expression of *tal1* in the absence of *npas4l*,
479 we injected *npas4l* mutant embryos with *npas4l* RNA or with *arnt1* and *arnt2* RNA (**Figure 5D-F)**.

480 Embryos injected with *npas4l* mRNA exhibited robust expression of *tal1* (**Figure 5E**), consistent with
481 previously published results (Reischauer et al., 2016). However, all the embryos (derived from
482 *npas4l*$^{s5/+}$ parents crossed to each other) injected with *arnt1* and *arnt2* mRNA showed little to no
483 expression of *tal1* (**Figure 5F**). Since 25% of these embryos are *npas4l*$^{s5/s5}$, we conclude that *arnt1* and
484 *arnt2* cannot drive *tal1* expression in the absence of *npas4l*. Finally, to test if *npas4l* upregulates target
485 genes in the absence of *arnt1* and *arnt2*, we injected *arnt1/2* mutant embryos with *npas4l* mRNA. We
486 found that *arnt1/2* siblings showed upregulation of *npas4l*-target gene *lmo2*, but *arnt1/2* mutants did not
487 show upregulation of *lmo2* (**Figure 5G-H**). From these results, we conclude that expression of *npas4l*
488 and either *arnt1* or *arnt2* are required for upregulation of *npas4l*-target genes.
489

490 **Npas4l interacts with both Arnt1 and Arnt2**

491 Npas4l is a Class I bHLH-PAS domain transcription factor (Reischauer et al., 2016), and as
492 such, must heterodimerize with a Class II bHLH-PAS transcription factor, like Arnt1 and Arnt2, to
493 regulate gene transcription. Considering that (1) bHLH-PAS transcription factors function as dimers, (2)
494 *arnt1* and *arnt2* fail to upregulate hemato-vascular genes in the absence of *npas4l*, and (3) *npas4l* fails
495 to upregulate hemato-vascular genes in *arnt1/2* mutants, therefore we hypothesize that Arnt1 and Arnt2
496 proteins form a transcription complex with Npas4l protein to regulate gene expression. To determine if
497 Npas4l interacts with Arnt1 or Arnt2, we performed a coimmunoprecipitation experiment. Due to the
498 absence of commercially available antibodies that recognize zebrafish Npas4l, Arnt1 or Arnt2 proteins,
499 we co-expressed tagged versions of zebrafish *npas4l* (Npas4l-V5), *arnt1* (Arnt1-myc), and *arnt2* (Arnt2-
500 HA) in HEK293T cells. We performed co-immunoprecipitation studies and found that Arnt1-myc
501 interacts with Npas4l-V5 and that Arnt2-HA interacts with Npas4l-V5 (**Figure 6**, N= 2 biological
502 replicates per condition). These results suggest that Npas4l uses either Arnt1 or Arnt2 or both as
503 binding partners. Furthermore, these data indicate that Arnt1 and Arnt2 may be functionally
504 interchangeable and redundant, at least in the case of Npas4l.

505

506 **Arnt1 and Arnt2 cannot functionally compensate for one another in the case of Ahr2**

507 Our results demonstrate that Arnt1 and Arnt2 are functionally interchangeable and redundant
508 when interacting with Npas4l in the context of hemato-vascular development. It is unclear if Arnt1 and
509 Arnt2 are functionally interchangeable with all Class I bHLH-PAS domain transcription factors or just
510 with Npas4l. To determine if *arnt1/arnt2* redundancy is unique to Npas4l, we examined if *arnt1* and
511 *arnt2* are interchangeable with a different class I bHLH-PAS transcription factor, the aryl hydrocarbon
512 receptor 2 (Ahr2). Previous studies demonstrate that Ahr2 can bind DNA in the presence of either Arnt1
513 or Arnt2 *in vitro* (Andreasen et al., 2002; Hirose et al., 1996; Tanguay et al., 2000), but whether Arnt1
514 and Arnt2 bind Ahr2 interchangeably *in vivo* is not known. Ahr2 is a ligand-dependent transcription
515 factor. A known ligand of Ahr2 is 2,3,7,8-tetrachlorodibenzo-p-dioxin (TCDD), which we have previously
516 shown induces cardiotoxicity in zebrafish larvae and requires *ahr2* (Souder and Gorelick, 2019). We
517 asked whether TCDD causes cardiotoxicity in *arnt1* or *arnt2* single mutants, reasoning that if Ahr2
518 interacts with Arnt1 or Arnt2 interchangeably, then only *arnt1/2* double mutants, but not single mutants,
519 would be resistant to TCDD exposure. We treated clutches of larvae from wild-type parents (N= 3
520 biological replicates, 10-60 larvae per clutch per drug treatment, 157 larvae total), *arnt1* heterozygous
521 parents (N= 3-4 biological replicates per allele, 21-36 larvae per clutch per drug treatment, 533 larvae
522 total, 248 larvae from allele *bcm1* and 285 larvae allele from *bcm2*), or *arnt2* heterozygous parents
523 (N=3 biological replicates, 40-45 embryos per clutch per drug treatment, 253 larvae total) with either
524 0.1% DMSO (vehicle) or with 10 ng/mL TCDD from 1 dpf to 3 dpf **(Figure S4)**. Wild-type larvae
525 exposed to TCDD exhibited pericardial edema and abnormal heart looping, consistent with previous
526 results (**Figure 7A, D)**. *arnt2* mutants treated with TCDD exhibited a phenotype similar to wild-type
527 (**Figure 7C, F)**. In contrast, *arnt1* mutants treated with TCDD showed normal heart looping and no
528 pericardial edema, similar to vehicle-treated larvae (**Figure 7B, E)**. This demonstrates that *arnt1,* but
529 not *arnt2,* is required for Ahr2-dependent TCDD toxicity. We conclude that *arnt1* and *arnt2* are not

530 always functionally redundant *in vivo*. Certain Class I bHLH-PAS transcription factors may prefer to

531 function with a specific Class II bHLH-PAS transcription faction.

532

533 **DISCUSSION**

534 We find that Arnt1 and Arnt2 are obligate coregulators of Npas4l. Together, *npas4l*, *arnt1* and *arnt2*
535 genes regulate specification of hemato-vascular cells. *npas4l*, *arnt1* and *arnt2* are each necessary, but
536 on their own not sufficient, for hemato-vascular specification. Npas4l serves as a master regulator, with
537 Arnt proteins acting as permissive coregulators. Arnt1 and Arnt2 are functionally redundant in the case
538 of Npas4l but are not functionally redundant in the case of Ahr2, where there is a preference for Ahr2-
539 Arnt1 complex.

540 Class I bHLH-PAS proteins must dimerize with Class II bHLH-PAS proteins to transcribe their target
541 genes (Card et al., 2005; Ema et al., 1996; Hirose et al., 1996; Jiang et al., 1996; Lees and Whitelaw,
542 1999; Michaud et al., 2000; Wu and Rastinejad, 2017). It has previously been established that Npas4l, a
543 Class I bHLH-PAS transcription factor, is required for hemato-vascular development in zebrafish
544 (Reischauer et al., 2016). To determine the Class II bHLH-PAS binding partner of Npas4l, we
545 generated *arnt1* mutant and *arnt2* mutant zebrafish and expected one of these mutants to mimic the
546 *npas4l* mutant phenotype. However, both *arnt1* mutant and *arnt2* single mutant larvae were viable to 5
547 dpf and were grossly indistinguishable from wild-type embryos. Only *arnt1/2* double mutant embryos
548 exhibited a cardiovascular phenotype. Our results demonstrate that double homozygous *arnt1/2* mutant
549 embryos have a similar phenotype to *npas4l* mutants (Reischauer et al., 2016; Stainier et al., 1995;
550 Thompson et al., 1998) and that Npas4l can function with either Arnt1 or Arnt2. Thus, Arnt1 and Arnt2
551 act redundantly to specify hemato-vascular progenitor cells in zebrafish.

552 Are *arnt1* and *arnt2* functionally redundant with all Class I bHLH-PAS transcription factors? We
553 argue no. In the case of the class I transcription factor Ahr2, both Arnt1 and Arnt2 bind Ahr2 *in vitro*
554 (Lanham et al., 2011; Tanguay et al., 2000). However, we find that only Arnt1, and not Arnt2, is required
555 for Ahr2-dependent cardiotoxicity in zebrafish embryos. This argues that *in vivo*, Ahr2 preferentially
556 interacts with Arnt1 over Arnt2. Another class I protein, Sim1a, appears to preferentially interact with
557 Arnt2 *in vivo*. *arnt2* mutant zebrafish embryos have fewer dopaminergic neurons in the brain compared
558 to wild-type embryos (Löhr et al., 2009). The *arnt2* mutant phenotype is similar to the phenotype when

559 Sim1a expression is knocked down (Löhr et al., 2009). These results suggest that in the case of the
560 growth and/or survival of dopaminergic neurons, Sim1a preferentially interacts with Arnt2 versus Arnt1.
561 To what degree this is due to differences in expression levels, versus an intrinsic structural preference
562 for a particular protein-protein interaction, requires further study. Such interactions may also depend on
563 the cell-type and developmental stage where the bHLH-PAS proteins function. Arnt1 and Arnt2 appear
564 to be expressed ubiquitously during embryonic development, which suggests that such interactions
565 may be due to factors other than expression levels.

566 Endothelial cell development and hematopoietic cell development are closely related during
567 embryogenesis. Both cell types primarily arise from the lateral plate mesoderm (LPM) and share a
568 common progenitor (Qian et al., 2005; Reischauer et al., 2016; Stainier et al., 1995; Thompson et al.,
569 1998). Additionally, during definitive hematopoiesis, some HSCs are derived from specialized
570 endothelial cells, called hemogenic endothelium (Boisset et al., 2010; Kissa and Herbomel, 2010). Both
571 *npas4l* and *arnt1/2* mutants lack all blood cells but do have a small population of endothelial cells,
572 which is restricted to the most posterior region of the animal (Figure 2 and (Reischauer et al., 2016)). In
573 zebrafish, there is a population of endothelial cells in the caudal region of the embryo that are not
574 derived from the LPM and differentiate in the absence of *npas4l* expression (Pak et al., 2020). We
575 hypothesize that *arnt1* and *arnt2* are required for the differentiation of endothelial cells from the LPM
576 but are not required for the differentiation of endothelial cells, such as the caudal population, from
577 outside the LPM. The transcriptomic signature of the caudal population of endothelial cells was distinct
578 from endothelial cells that require *npas4l* for differentiation, with genes for somitogenesis and
579 neurogenesis highly enriched compared to LPM-derived endothelial cells (Pak et al., 2020). Based on
580 this transcriptome analysis, we speculate that the caudal population of endothelial cells fails to express
581 genes required for hemogenic endothelium and that no blood cells are derived from the caudal
582 population of endothelial cells. This is consistent with the observation that the caudal population of
583 endothelial cells, but not blood cells, are present in *npas4l* or *arnt1/2* mutants.

584 Arnt proteins interact with multiple class I bHLH-PAS domain proteins to regulate cardiovascular
585 development. Our results focused on the role of Arnt proteins in hemato-vascular specification,
586 however Arnt proteins are likely involved in later steps of endothelial cell development. Differentiation of
587 hemogenic endothelium in zebrafish and in mice is dependent upon several Class I bHLH-PAS
588 transcription factors: Hypoxia inducible factor 1 alpha (mouse *Hif1α*, zebrafish genes *hif1aa*, *hif1ab)*
589 and hypoxia inducible factor 2 alpha (mouse *Hif2α,* zebrafish genes *epas1a*, *epas1b*) (Gerri et al., 2018;
590 Ramírez-Bergeron et al., 2004). Given that these HIF proteins are Class I bHLH-PAS transcription
591 factors, it is likely that one or both Arnt proteins are required for HIF-dependent differentiation of
592 hemogenic endothelium.
593 The function of Arnt proteins in zebrafish cardiovascular development is likely conserved in mice.
594 Arnt1 is essential for the viability of adult hematopoietic stem cells in mice and is required for the
595 survival of hematopoietic progenitor cells in the fetal mouse liver (Krock et al., 2015). Homozygous
596 *Arnt1* mutant mice are not viable beyond E10.5 and show severe defects in vascularization, suggesting
597 that Arnt1 is essential for normal vascular development (Kozak et al., 1997; Maltepe et al., 1997). The
598 degree to which Arnt2 contributes to hemato-vascular development in mice is not well-understood.
599 Arnt2 has primarily been studied within the context of neural development (Hao et al., 2013; Hosoya et
600 al., 2001; Jain et al., 1998), however, there is some evidence to suggest that *Arnt1* and *Arnt2* may
601 exhibit functional redundancy during development of non-neural tissues (Keith et al., 2001; Sekine et
602 al., 2006). We observed lower than expected numbers of *arnt1*$^{bcm2/bcm2}$*; arnt2*$^{bcm3/+}$ adult zebrafish
603 derived from *arnt1*$^{bcm2/+}$*; arnt2*$^{bcm3/+}$ parents. This suggests that *arnt1* and *arnt2* have a dose-dependent
604 effect on the survival or fitness of the animal, where anything less than four wild-type alleles (two *arnt1*
605 alleles, two *arnt2* alleles) is deleterious. A similar dose-dependent effect on survival can be seen in
606 mouse embryos from *Arnt1*$^{+/-}$*;Arnt2*$^{+/-}$ parents (Keith et al., 2001). The mechanisms behind these dose-
607 dependent gene effects are not known.
608 While zebrafish *arnt1* and *arnt2* genes are conserved in mammals, there is no known equivalent of
609 zebrafish *npas4l* in mammalian genomes. Zebrafish Npas4l shows the highest sequence homology to

610 mouse Npas4 (Reischauer et al., 2016). Although Npas4 is known to dimerize with Arnt1 and Arnt2 *in*
611 *vivo* (Brigidi et al., 2019), mammalian Npas4 is unlikely to be the functional equivalent to zebrafish
612 Npas4l because homozygous Npas4 mutant mice are viable to adulthood and do not show any overt
613 vascular or hematopoietic defects (Bloodgood et al., 2013). Given our results that *npas4l* requires *arnt1*
614 or *arnt2* to act as co-regulators of hemato-vascular specification, and the abundance of conserved
615 genes that regulate vascular development in zebrafish and humans (Hogan and Schulte-Merker, 2017),
616 we speculate that the functional mammalian equivalent of *npas4l* is a Class I bHLH-PAS transcription
617 factor, or multiple such factors, that function together with Arnt1 or Arnt2.
618

619 **Acknowledgements**

620 We thank Lauren Pandolfo and the staff of the Baylor College of Medicine aquatics facility for taking
621 care of our zebrafish colony, Rosa Uribe and Adam Howard from Rice University for help with WIHCR,
622 and Paula Pimienta-Ramirez and Yunping Lei in the CPEH DNA sequencing core at BCM for help with
623 sequencing embryos following in situ hybridization. This work was supported by NIH grants
624 R01ES026337 (to DAG), P30ES030285 (pilot award to DAG), and T32DK060445 (to MJE).
625

626

627
628

Genotype	***Expected Percentage***	***Expected*** *n=356*	***Actual Percentage***	***Actual*** *n=356*
arnt1$^{+/+}$*; arnt2*$^{+/+}$	6.3%	22.25	6.2%	22
arnt1$^{+/+}$*; arnt2*$^{bcm3/+}$	12.5%	44.5	14.3%	51
arnt1$^{+/+}$*; arnt2*$^{bcm3/bcm3}$	6.3%	22.25	4.5%	16
arnt1$^{bcm2/+}$*; arnt2*$^{+/+}$	12.5%	44.5	11.8%	42
arnt1$^{bcm2/+}$*; arnt2*$^{bcm3/+}$	25%	89	25.3%	90
arnt1$^{bcm2/+}$*; arnt2*$^{bcm3/bcm3}$	12.5%	44.5	11.8%	42
arnt1$^{bcm2/bcm2}$*; arnt2*$^{+/+}$	6.3%	22.25	5.3%	19
arnt1$^{bcm2/bcm2}$*; arnt2*$^{bcm3/+}$	12.5%	44.5	13.5%	48
arnt1$^{bcm2/bcm2}$*; arnt2*$^{bcm3/bcm3}$	6.3%	22.25	7.3%	26

Table 1. Genotypes of embryos from *arnt1*$^{bcm2/+}$*; arnt2*$^{bcm3/+}$ parents follow expected Mendelian ratios. The frequencies of the observed genotypes were not significantly different from the expected genotypes, X^2 (8, N=356) = 4.38, p>0.05.

631

Genotype	Expected Percentage	Expected n=138	Actual Percentage	Actual n=138
arnt1$^{+/+}$; *arnt2*$^{+/+}$	7.69%	10.6	7.24%	10
arnt1$^{+/+}$; *arnt2*$^{bcm3/+}$	15.4%	21.25	15.2%	21
arnt1$^{+/+}$; *arnt2*$^{bcm3/bcm3}$	0%	0	0%	0
arnt1$^{bcm2/+}$; *arnt2*$^{+/+}$	13.3%	18.4	30.4%	42
arnt1$^{bcm2/+}$; *arnt2*$^{bcm3/+}$	30.8%	42	43.5%	60
arnt1$^{bcm2/+}$; *arnt2*$^{bcm3/bcm3}$	0%	0	0%	0
arnt1$^{bcm2/bcm2}$; *arnt2*$^{+/+}$	7.69%	10.6	1.45%	2
arnt1$^{bcm2/bcm2}$; *arnt2*$^{bcm3/+}$	15.4%	21.25	2.17%	3
arnt1$^{bcm2/bcm2}$; *arnt2*$^{bcm3/bcm3}$	0%	0	0%	0

632
633

Table 2. Genotype frequencies of viable adult fish from *arnt1*$^{bcm2/+}$; *arnt2*$^{bcm3/+}$ parents. Offspring were raised to adulthood (≥3 months old) and genotyped. The expected Mendelian ratios were adjusted to reflect the fact that *arnt2*$^{bcm3/bcm3}$ mutants are not viable to adulthood. The frequencies of the observed genotypes were significantly different from the expected genotypes, with fewer *arnt1*$^{bcm2/bcm2}$; *arnt2*$^{bcm3/+}$ observed. X^2 (5, N=138) = 45.57, p<0.0001.

634 **Figure 1. *arnt1*/2 double mutant embryos, but not *arnt1* or *arnt2 single* mutants, lack circulating**
635 **blood, have cardiac edema and atrial enlargement. (A)** bHLH-PAS transcription factors act as
636 heterodimers: a Class I protein and Class II protein interact and bind DNA. Asterisks indicate proteins
637 encoded by genes present in zebrafish but absent in humans. (**B,C**) Generation of zebrafish with
638 mutations in *arnt1* and *arnt2* genes. The amino acid sequences for the zebrafish Arnt1 (**B**), and Arnt2
639 proteins (**C**) are represented by the black line. Basic helix-loop-helix (bHLH), Per-Arnt-Sim (PAS)
640 domains, and the motif C-terminally located to the PAS (PAC) are represented by the labeled bubbles.
641 The numbers below each domain indicate the starting and ending amino acid (AA) for each motif. (**B**)
642 The *arnt1*^{bcm1} mutation causes a premature stop codon to occur at AA139 and loss of the PAS-B, PAC,
643 and majority of the PAS-A. The *arnt1*^{bcm2} mutation causes a premature stop codon to occur at AA250
644 and loss of the PAS-B and PAC domains. (**C**) The *arnt2*^{bcm3} mutation causes a premature stop codon to
645 occur at AA287 and loss of the PAS-B and PAC domains. (**D-I**) Live images of embryos from the
646 indicated genotype at 2 days post fertilization (dpf). All double homozygous *arnt1*$^{bcm2/bcm2}$*; arnt2*$^{bcm3/bcm3}$
647 embryos showed cardiac edema and atrial enlargement (**G** and **G'**). The wildtype (**D** and **D'**),
648 *arnt1*$^{bcm2/bcm2}$ (**E** and **E'**), and *arnt2*$^{bcm3/bcm3}$ (**F** and **F'**) siblings of the double homozygous mutants
649 (*arnt1*$^{bcm2/bcm2}$*; arnt2*$^{bcm3/bcm3}$) showed normal heart development. Black arrows in panels D'-G' indicate
650 the atrium and ventricle of the heart. Images are representative of 7 different clutches, each clutch
651 contained 20-300 embryos. All siblings of double homozygous mutants (*arnt1*$^{bcm2/bcm2}$*; arnt2*$^{bcm3/bcm3}$)
652 had circulating blood (**H** and **Movie 1, Movie 2, Movie 5, Movie 6**) while *arnt1/2* mutants lacked visible
653 circulating blood cells (**I** and **Movie 3, Movie 4, Movie 7, Movie 8**). The black arrows in panel **H**
654 indicate blood cells. The arrowheads in **H** and **I** indicate non-blood cells found in all embryos. (**J-L**), o-
655 dianisidine staining to label blood cells in embyos 3 days post fertilization shows that *arnt1*$^{bcm2/bcm2}$;
656 *arnt2*$^{bcm3/bcm3}$ double homozygous mutants lack blood cells, while all other genotypes have clearly
657 labeled blood cells. The arrow in **J** and **K** points to the duct of Cuvier, and the arrowheads in **K** show
658 circulating blood cells. All embryos were derived from *arnt1*$^{bcm2/+}$*;arnt2*$^{bcm3/+}$ parents, images are
659 representative of 1 clutch, containing 98 embryos. (**J**) N=96 of 98 embryos showed clear o-dianisidine
660 staining and none of these embryos were *arnt1/2* mutants. (**K**) N=2 of 98 embryos showed a lack of o-
661 dianisidine staining and both embryos were confirmed *arnt1/2* mutants. For all images anterior is
662 towards the left and dorsal is towards the top, except for panel **J** which shows a ventral view of the
663 embryos. Scale bars: D-G, 1 mm; D'-G' and H-K, 100 µm.
664

665 **Figure 2. *arnt1/2* mutants show reduced levels of endothelial cells and *runx1*-positive**
666 **hematopoietic cells. (A-L)** Embryos were probed for *kdrl* (A-D) or *runx1* (E-H) using whole-mount in
667 situ hybridization at 2 days post fertilization (dpf). (A-D) *kdrl* staining in wild-type, *arnt1* mutant, *arnt2*

668 mutant, and *arnt1/2* mutant embryos. (A'-D') Images of each embryo's trunk near the end of the yolk
669 extension (indicated by the box in panels A-D). Black arrowheads indicate *kdrl* staining in the dorsal
670 longitudinal anastomotic vessels, black arrows indicate the dorsal aorta and caudal vein, and white
671 arrowheads indicate inter-segmental vessels. (E-H) Black arrows indicate *runx1* labeling in the
672 presumptive hematopoietic stem cell niche. (I-L) Wild-type and mutant embryos on Tg(*fli1:EGFP* ^{y1})
673 transgenic background were imaged at 1 dpf and then genotyped. (I'-L') Enlarged images of each
674 embryo's trunk near the end of the yolk extension (indicated by the box in panels I-L). White
675 arrowheads correspond to inter-segmental vessels. e: eye, pa: pharyngeal arch, da: dorsal aorta, cv:
676 caudal vein. The fraction in the bottom right corner indicates the number of embryos of the given
677 genotype with the represented phenotype over the total number of embryos of the given genotype from
678 a single clutch. Scale bars,100 μm.
679
680 **Figure 3. *arnt1/2* mutants show decreased *etsrp*, *tal1*, and *lmo2* expression in the lateral plate**
681 **mesoderm at 4-6 somite stages.** Whole-mount in situ hybridization for *etsrp*, *tal1,* and *lmo2*
682 expression was performed on 4-6 somite stage embryos that were offspring of *arnt1*$^{bcm2/+}$*;arnt2*$^{bcm3/+}$
683 adult zebrafish. (**A**) Expression of *etsrp* was observed in the anterior and posterior lateral plate
684 mesoderm (ALPM, PLPM) in 93% of embryos. (**B**) Limited or no expression of *etsrp* was observed in
685 7% of embryos, consistent with the expected Mendelian ratio of 6.25% for *arnt1*$^{bcm2/+}$*;arnt2*$^{bcm3/+}$ (*arnt1/2*
686 mutants). (**C**) Expression of *tal1* was observed in the ALPM and PLPM in 93% of embryos. (**D**) Limited
687 or no expression of *tal1* was observed in 7% of embryos, consistent with the expected Mendelian ratio
688 of 6.25% for *arnt1/2* mutants. (**E**) Expression of *lmo2* was observed in 89% of embryos. (**F**) Limited or
689 no expression of *lmo2* was observed in 11% of embryos, which is slightly more than the expected
690 Mendelian ratio of 6.25% for *arnt1/2* mutants. We genotyped a subset of each group of embryos (see
691 **Supplemental Tables 2-4**) and observed a correlation between number of mutant alleles and
692 expression of *etsrp*, *tal1*, and *lmo2* genes. Spearman correlation, *etsrp* r= -0.9, p<0.001; *tal1* r= -0.6,
693 p<0.005; *lmo2* r= -0.2, p<0.01. All embryos are oriented with dorsal towards the top. Fractions in
694 bottom right corners refer to the number of embryos with the indicated phenotype over the total number
695 of embryos examined. Scale bars, 100 μm
696
697 **Figure 4. *arnt1* and *arnt2* are ubiquitously expressed at the 4-somite stage and co-localized with**
698 ***npas4l* expression.** Whole-mount *in situ* hybridization chain reaction was performed on wild-type (AB)
699 embryos at the 4 somite stage. (**A**) Embryos were probed for *npas4l, arnt1,* and *arnt2* expression and
700 counter-stained with DAPI. *arnt1* and *arnt2* labeling was detected ubiquitously, while *npas4l* labeling
701 was localized to the lateral plate mesoderm. (A') Higher magnification views of the boxed areas in (A)

shows co-localization of *arnt1, arnt2,* and *npas4l* in the posterior lateral plate mesoderm, outlined in cyan. (**B**) To demonstrate that the observed expression of *arnt1* and *arnt2* is not autofluorescence of the embryo or the yolk, wild-type embryos were processed identically to those in (A), but no anti-sense RNA probe sets were added. (B') Higher magnification views of the boxed areas in (B) shows what background/autofluorescence looks like in the presumptive posterior lateral plate mesoderm. All images in (**A, B**) are maximum intensity projections from z-stacks taken every 2.5 μm. In merged panels, *npas4l* is green, *arnt1* is magenta, *arnt2* is cyan. The posterior portion of the embryo is in view, dorsal is towards the top of the image. Scale bars, 100 μm. (**C-E**) To validate the observed expression of *arnt1* and *arnt2,* we quantified the number of detectable objects above a set threshold in the whole embryo across each z-plane for 4 negative control embryos and 6 experimental embryos probed for *arnt1*, *arnt2* and *npas4l*. We then normalized the number of detected objects by subtracting the average number of objects detected in the negative controls from the number of detected objects in the experimental embryos. Each point on these graphs represents the total number of objects above threshold for a single embryo. (**F-H**) To demonstrate that *arnt1* and *arnt2* expression occurs in the lateral plate mesoderm (LPM), we calculated the integrated intensity of fluorescence (pixel area, pixel intensity) over each side of the posterior LPM in maximum intensity projections from control and experimental embryos. Each point represents the integrated intensity from one side of the posterior LPM from a single embryo (right or left side), where each embryo has two bilateral *npas4l*-positive regions of the posterior LPM. Points of the same color are measurements from opposite sides of the posterior LPM from the same embryo. *npas4l*, *arnt1*, and *arnt2* labeling was statistically significantly increased in the lateral plate mesoderm compared to negative control embryos. *npas4l* Welch's t-test, $t(11)=8.6$, $p<0.0001$; *arnt1* Mann-Whitney, $U=0$, $p<0.0001$; *arnt2* Welch's t-test, $t(11)=7.0$, $p<0.0001$

Figure 5. Expression of *npas4l*-target genes requires *npas4l*, *arnt1* and *arnt2*. Zebrafish embryos, derived from the indicted parental genotypes, were injected at the one-cell stage with 50 pg of *npas4l* mRNA or with 50 pg each of *arnt1* and *arnt2* mRNA (100 pg total RNA). Embryos were fixed at shield stage and probed for *tal1* or *lmo2, npas4l*-target genes, using whole mount in situ hybridization. Embryos were then genotyped. (A-C) In wild-type embryos, *tal1* is expressed following injection of *npas4l* RNA. *tal1* mRNA was not detected in uninjected embryos or following injection of *arnt1* and *arnt2* RNA. (D-F) Heterozygous *npas4l* mutant fish were crossed to each other and the resulting embryos were injected with the indicated RNA. *npas4l* RNA, but not *arnt1* and *arnt2* RNA, upregulated expression of *tal1*. Genotype of embryos in (E) n = 11 $npas4l^{+/+}$, n = 15 $npas4l^{s5/+}$, n = 10 $npas4l^{s5/s5}$, (F) n = 12 $npas4l^{+/+}$, n = 20 $npas4l^{s5/+}$, n = 8 $npas4l^{s5/s5}$. (G-I) $arnt1^{bcm2/+};arnt2^{bcm3/+}$ adults were crossed to each other and the resulting embryos were injected with *npas4l* RNA. Double homozygous embryos

failed to upregulate *lmo2* (panel I) whereas sibling embryos upregulated *lmo2* (H). Genotype of embryos in (H) n = 1 *arnt1*$^{+/+}$*;arnt2*$^{+/+}$, n = 7 *arnt1*$^{bcm2/+}$*;arnt2*$^{bcm3/+}$, n = 1 *arnt1*$^{+/+}$*;arnt2*$^{bcm3/+}$, n = 8 *arnt1*$^{bcm2/+}$*;arnt2*$^{+/+}$, n= 4 *arnt1*$^{+/+}$*;arnt2*$^{bcm3/bcm3}$, n= 7 *arnt1*$^{bcm2/bcm2}$*;arnt2*$^{+/+}$, n = 7 *arnt1*$^{bcm2/+}$*;arnt2*$^{bcm3/bcm3}$, n = 4 *arnt1*$^{bcm2/bcm2}$*;arnt2*$^{bcm3/+}$, (I) n = 3 *arnt1*$^{bcm2/bcm2}$*;arnt2*$^{bcm3/bcm3}$. Embryos are oriented in a lateral view with the animal pole towards the top. Fractions in the bottom right corner indicate the number of embryos with the represented phenotype over the total number of embryos assayed. Scale bar in (A) applies to all panels, 100 μm.

Figure 6. Arnt1 and Arnt2 co-immunoprecipitate with Npas4l. (A) HEK293T cells were transfected with zebrafish Npas4l-V5 and Arnt1-myc. Cells were homogenized (input) and immunoprecipitated (IP) with antibodies against V5 or an immunoglobulin G control (IgG). Samples were run on an immunoblot and probed using myc antibodies (anti-myc) to detect the presence of Arnt1-myc (top) or samples were probed using V5 antibodies (anti-V5) to verify successful pulldown of Npas4l-V5 (bottom). **(B)** HEK293T cells were transfected with zebrafish Npas4l-V5 and Arnt2-HA. Cells were homogenized and immunoprecipitated with antibodies against HA or an IgG control. Samples were run on an immunoblot and probed using V5 antibodies (anti-V5) to detect the presence of Npas4l-V5 (top) or samples were probed using HA antibodies (anti-HA) to verify successful pulldown of Arnt2-HA (bottom).

Figure 7. Mutation in *arnt1,* but not *arnt2,* prevents AHR2-dependent TCDD toxicity. Wild-type or mutant larvae were exposed to (**A, B, C**) 0.1% DMSO, or (**D, E, F**) 2,3,7,8-tetrachlorodibenzodioxin (TCDD) from 1-3 dpf and imaged at 3 dpf. (**A, D**) Wildtype larvae exposed to TCDD lack an S-shaped cardiac loop and exhibit cardiac edema, unlike vehicle treated wild-type siblings. (**B,E**) *arnt1* mutant larvae (*arnt1*$^{bcm2/bcm2}$) treated with vehicle and TCDD show normal heart looping and do not have cardiac edema. (**C,F**) *arnt2* mutant larvae (*arnt2*$^{bcm3/bcm3}$) treated with vehicle show expected heart looping similar to wild type siblings, but *arnt2* homozygous mutant larvae treated with TCDD lack an S-shaped cardiac loop similar to wild type and exhibit cardiac edema similar to TCDD treated wild-type larvae. Black arrows indicate location of the heart. Larvae were genotyped following imaging and representative images are shown. TCDD treated wild-type siblings of *arnt1* mutant larvae, n= 9 larvae across 3 clutches; TCDD treated *arnt1* mutant larvae, n=21 larvae across 3 clutches. TCDD treated wild-type siblings of *arnt2* larvae, n=19 larvae across 3 clutches; TCDD treated *arnt2* mutant larvae, n=22 larvae across 4 clutches. All larvae are oriented with anterior to the left and dorsal towards the top. Scale bar, 100 μm.

Andreasen, E. A., Spitsbergen, J. M., Tanguay, R. L., Stegeman, J. J., Heideman, W. and Peterson, R. E. (2002). Tissue-specific expression of AHR2, ARNT2, and CYP1A in zebrafish embryos and larvae: effects of developmental stage and 2,3,7,8-tetrachlorodibenzo-p-dioxin exposure. *Toxicol. Sci.* **68**, 403–419.

Baranasic, D., Hörtenhuber, M., Balwierz, P. J., Zehnder, T., Mukarram, A. K., Nepal, C., Várnai, C., Hadzhiev, Y., Jimenez-Gonzalez, A., Li, N., et al. (2022). Multiomic atlas with functional stratification and developmental dynamics of zebrafish cis-regulatory elements. *Nat. Genet.* **54**, 1037–1050.

Begley, C. G., Aplan, P. D., Denning, S. M., Haynes, B. F., Waldmann, T. A. and Kirsch, I. R. (1989). The gene SCL is expressed during early hematopoiesis and encodes a differentiation-related DNA-binding motif. *Proc Natl Acad Sci USA* **86**, 10128–10132.

Bloodgood, B. L., Sharma, N., Browne, H. A., Trepman, A. Z. and Greenberg, M. E. (2013). The activity-dependent transcription factor NPAS4 regulates domain-specific inhibition. *Nature* **503**, 121–125.

Boisset, J.-C., van Cappellen, W., Andrieu-Soler, C., Galjart, N., Dzierzak, E. and Robin, C. (2010). In vivo imaging of haematopoietic cells emerging from the mouse aortic endothelium. *Nature* **464**, 116–120.

Bolte, S. and Cordelières, F. P. (2006). A guided tour into subcellular colocalization analysis in light microscopy. *J. Microsc.* **224**, 213–232.

Brigidi, G. S., Hayes, M. G. B., Delos Santos, N. P., Hartzell, A. L., Texari, L., Lin, P.-A., Bartlett, A., Ecker, J. R., Benner, C., Heinz, S., et al. (2019). Genomic Decoding of Neuronal Depolarization by Stimulus-Specific NPAS4 Heterodimers. *Cell* **179**, 373-391.e27.

Card, P. B., Erbel, P. J. A. and Gardner, K. H. (2005). Structural basis of ARNT PAS-B dimerization: use of a common beta-sheet interface for hetero- and homodimerization. *J. Mol. Biol.* **353**, 664–677.

Casie Chetty, S., Rost, M. S., Enriquez, J. R., Schumacher, J. A., Baltrunaite, K., Rossi, A., Stainier, D. Y. R. and Sumanas, S. (2017). Vegf signaling promotes vascular endothelial differentiation by modulating etv2 expression. *Dev. Biol.* **424**, 147–161.

Dooley, K. A., Davidson, A. J. and Zon, L. I. (2005). Zebrafish scl functions independently in hematopoietic and endothelial development. *Dev. Biol.* **277**, 522–536.

Dumont, D. J., Fong, G. H., Puri, M. C., Gradwohl, G., Alitalo, K. and Breitman, M. L. (1995). Vascularization of the mouse embryo: a study of flk-1, tek, tie, and vascular endothelial growth factor expression during development. *Dev. Dyn.* **203**, 80–92.

Edwards, H. E. and Gorelick, D. A. (2022). The evolution and structure/function of bHLH-PAS transcription factor family. *Biochem. Soc. Trans.* **50**, 1227–1243.

Ema, M., Morita, M., Ikawa, S., Tanaka, M., Matsuda, Y., Gotoh, O., Saijoh, Y., Fujii, H., Hamada, H., Kikuchi, Y., et al. (1996). Two new members of the murine Sim gene family are transcriptional

809 repressors and show different expression patterns during mouse embryogenesis. *Mol. Cell. Biol.* **16**,
810 5865–5875.

811 **Ferrara, N., Carver-Moore, K., Chen, H., Dowd, M., Lu, L., O'Shea, K. S., Powell-Braxton, L.,**
812 **Hillan, K. J. and Moore, M. W.** (1996). Heterozygous embryonic lethality induced by targeted
813 inactivation of the VEGF gene. *Nature* **380**, 439–442.

814 **Gerri, C., Marass, M., Rossi, A. and Stainier, D. Y. R.** (2018). Hif-1α and Hif-2α regulate hemogenic
815 endothelium and hematopoietic stem cell formation in zebrafish. *Blood* **131**, 963–973.

816 **Hao, N., Bhakti, V. L. D., Peet, D. J. and Whitelaw, M. L.** (2013). Reciprocal regulation of the basic
817 helix-loop-helix/Per-Arnt-Sim partner proteins, Arnt and Arnt2, during neuronal differentiation. *Nucleic*
818 *Acids Res.* **41**, 5626–5638.

819 **Herbert, S. P. and Stainier, D. Y. R.** (2011). Molecular control of endothelial cell behaviour during
820 blood vessel morphogenesis. *Nat. Rev. Mol. Cell Biol.* **12**, 551–564.

821 **Hill, A. J., Heiden, T. C. K., Heideman, W. and Peterson, R. E.** (2009). Potential roles of Arnt2 in
822 zebrafish larval development. *Zebrafish* **6**, 79–91.

823 **Hirose, K., Morita, M., Ema, M., Mimura, J., Hamada, H., Fujii, H., Saijo, Y., Gotoh, O., Sogawa, K.**
824 **and Fujii-Kuriyama, Y.** (1996). cDNA cloning and tissue-specific expression of a novel basic helix-
825 loop-helix/PAS factor (Arnt2) with close sequence similarity to the aryl hydrocarbon receptor nuclear
826 translocator (Arnt). *Mol. Cell. Biol.* **16**, 1706–1713.

827 **Hirschi, K. K.** (2012). Hemogenic endothelium during development and beyond. *Blood* **119**, 4823–
828 4827.

829 **Hogan, B. M. and Schulte-Merker, S.** (2017). How to plumb a pisces: understanding vascular
830 development and disease using zebrafish embryos. *Dev. Cell* **42**, 567–583.

831 **Hosoya, T., Oda, Y., Takahashi, S., Morita, M., Kawauchi, S., Ema, M., Yamamoto, M. and Fujii-**
832 **Kuriyama, Y.** (2001). Defective development of secretory neurones in the hypothalamus of Arnt2-
833 knockout mice. *Genes Cells* **6**, 361–374.

834 **Huber, T. L., Kouskoff, V., Fehling, H. J., Palis, J. and Keller, G.** (2004). Haemangioblast
835 commitment is initiated in the primitive streak of the mouse embryo. *Nature* **432**, 625–630.

836 **Jain, S., Maltepe, E., Lu, M. M., Simon, C. and Bradfield, C. A.** (1998). Expression of ARNT, ARNT2,
837 HIF1?, HIF2? and Ah receptor mRNAs in the developing mouse. *Mech. Dev.* **73**, 117–123.

838 **Jiang, B. H., Rue, E., Wang, G. L., Roe, R. and Semenza, G. L.** (1996). Dimerization, DNA binding,
839 and transactivation properties of hypoxia-inducible factor 1. *J. Biol. Chem.* **271**, 17771–17778.

840 **Kafina, M. D. and Paw, B. H.** (2018). Using the zebrafish as an approach to examine the mechanisms
841 of vertebrate erythropoiesis. *Methods Mol. Biol.* **1698**, 11–36.

842 **Kalev-Zylinska, M. L., Horsfield, J. A., Flores, M. V. C., Postlethwait, J. H., Vitas, M. R., Baas, A.**
843 **M., Crosier, P. S. and Crosier, K. E.** (2002). Runx1 is required for zebrafish blood and vessel
844 development and expression of a human RUNX1-CBF2T1 transgene advances a model for studies
845 of leukemogenesis. *Development* **129**, 2015–2030.

846 **Kataoka, H., Hayashi, M., Nakagawa, R., Tanaka, Y., Izumi, N., Nishikawa, S., Jakt, M. L., Tarui, H.**
847 **and Nishikawa, S.-I.** (2011). Etv2/ER71 induces vascular mesoderm from Flk1+PDGFRα+ primitive
848 mesoderm. *Blood* **118**, 6975–6986.

849 **Keith, B., Adelman, D. M. and Simon, M. C.** (2001). Targeted mutation of the murine arylhydrocarbon
850 receptor nuclear translocator 2 (Arnt2) gene reveals partial redundancy with Arnt. *Proc Natl Acad Sci*
851 *USA* **98**, 6692–6697.

852 **Kissa, K. and Herbomel, P.** (2010). Blood stem cells emerge from aortic endothelium by a novel type
853 of cell transition. *Nature* **464**, 112–115.

854 **Kobayashi, I., Kobayashi-Sun, J., Kim, A. D., Pouget, C., Fujita, N., Suda, T. and Traver, D.** (2014).
855 Jam1a-Jam2a interactions regulate haematopoietic stem cell fate through Notch signalling. *Nature*
856 **512**, 319–323.

857 **Kozak, K. R., Abbott, B. and Hankinson, O.** (1997). ARNT-deficient mice and placental
858 differentiation. *Dev. Biol.* **191**, 297–305.

859 **Krock, B. L., Eisinger-Mathason, T. S., Giannoukos, D. N., Shay, J. E., Gohil, M., Lee, D. S.,**
860 **Nakazawa, M. S., Sesen, J., Skuli, N. and Simon, M. C.** (2015). The aryl hydrocarbon receptor
861 nuclear translocator is an essential regulator of murine hematopoietic stem cell viability. *Blood* **125**,
862 3263–3272.

863 **Lam, E. Y. N., Chau, J. Y. M., Kalev-Zylinska, M. L., Fountaine, T. M., Mead, R. S., Hall, C. J.,**
864 **Crosier, P. S., Crosier, K. E. and Flores, M. V.** (2009). Zebrafish runx1 promoter-EGFP transgenics
865 mark discrete sites of definitive blood progenitors. *Blood* **113**, 1241–1249.

866 **Lanham, K. A., Prasch, A. L., Weina, K. M., Peterson, R. E. and Heideman, W.** (2011). A dominant
867 negative zebrafish Ahr2 partially protects developing zebrafish from dioxin toxicity. *PLoS ONE* **6**,
868 e28020.

869 **Lawson, N. D. and Weinstein, B. M.** (2002). In vivo imaging of embryonic vascular development using
870 transgenic zebrafish. *Dev. Biol.* **248**, 307–318.

871 **Lees, M. J. and Whitelaw, M. L.** (1999). Multiple roles of ligand in transforming the dioxin receptor to
872 an active basic helix-loop-helix/PAS transcription factor complex with the nuclear protein Arnt. *Mol.*
873 *Cell. Biol.* **19**, 5811–5822.

874 **Lee, R. K., Stainier, D. Y., Weinstein, B. M. and Fishman, M. C.** (1994). Cardiovascular development
875 in the zebrafish. II. Endocardial progenitors are sequestered within the heart field. *Development* **120**,
876 3361–3366.

877 **Liao, W., Bisgrove, B. W., Sawyer, H., Hug, B., Bell, B., Peters, K., Grunwald, D. J. and Stainier,**
878 **D. Y.** (1997). The zebrafish gene cloche acts upstream of a flk-1 homologue to regulate endothelial
879 cell differentiation. *Development* **124**, 381–389.

880 **Liao, E. C., Paw, B. H., Oates, A. C., Pratt, S. J., Postlethwait, J. H. and Zon, L. I.** (1998). SCL/Tal-1
881 transcription factor acts downstream of cloche to specify hematopoietic and vascular progenitors in
882 zebrafish. *Genes Dev.* **12**, 621–626.

883 **Liao, W., Ho, C. Y., Yan, Y. L., Postlethwait, J. and Stainier, D. Y.** (2000). Hhex and scl function in
884 parallel to regulate early endothelial and blood differentiation in zebrafish. *Development* **127**, 4303–
885 4313.

886 **Löhr, H., Ryu, S. and Driever, W.** (2009). Zebrafish diencephalic A11-related dopaminergic neurons
887 share a conserved transcriptional network with neuroendocrine cell lineages. *Development* **136**,
888 1007–1017.

889 **Maltepe, E., Schmidt, J. V., Baunoch, D., Bradfield, C. A. and Simon, M. C.** (1997). Abnormal
890 angiogenesis and responses to glucose and oxygen deprivation in mice lacking the protein ARNT.
891 *Nature* **386**, 403–407.

892 **Marass, M., Beisaw, A., Gerri, C., Luzzani, F., Fukuda, N., Günther, S., Kuenne, C., Reischauer, S.**
893 **and Stainier, D. Y. R.** (2019). Genome-wide strategies reveal target genes of Npas4l associated with
894 vascular development in zebrafish. *Development* **146**,.

895 **Marchi, D., Santhakumar, K., Markham, E., Li, N., Storbeck, K.-H., Krone, N., Cunliffe, V. T. and**
896 **van Eeden, F. J. M.** (2020). Bidirectional crosstalk between Hypoxia-Inducible Factor and
897 glucocorticoid signalling in zebrafish larvae. *PLoS Genet.* **16**, e1008757.

898 **Mattonet, K., Riemslagh, F. W., Guenther, S., Prummel, K. D., Kesavan, G., Hans, S.,**
899 **Ebersberger, I., Brand, M., Burger, A., Reischauer, S., et al.** (2022). Endothelial versus
900 pronephron fate decision is modulated by the transcription factors Cloche/Npas4l, Tal1, and Lmo2.
901 *Sci. Adv.* **8**, eabn2082.

902 **Michaud, J. L., DeRossi, C., May, N. R., Holdener, B. C. and Fan, C. M.** (2000). ARNT2 acts as the
903 dimerization partner of SIM1 for the development of the hypothalamus. *Mech. Dev.* **90**, 253–261.

904 **North, T. E., Goessling, W., Peeters, M., Li, P., Ceol, C., Lord, A. M., Weber, G. J., Harris, J.,**
905 **Cutting, C. C., Huang, P., et al.** (2009). Hematopoietic stem cell development is dependent on blood
906 flow. *Cell* **137**, 736–748.

907 **Okuda, T., van Deursen, J., Hiebert, S. W., Grosveld, G. and Downing, J. R.** (1996). AML1, the
908 target of multiple chromosomal translocations in human leukemia, is essential for normal fetal liver
909 hematopoiesis. *Cell* **84**, 321–330.

910 **Pak, B., Schmitt, C. E., Choi, W., Kim, J.-D., Han, O., Alsiö, J., Jung, D.-W., Williams, D. R.,**
911 **Coppieters, W., Stainier, D. Y. R., et al.** (2020). Analyses of Avascular Mutants Reveal Unique
912 Transcriptomic Signature of Non-conventional Endothelial Cells. *Front. Cell Dev. Biol.* **8**, 589717.

913 **Palis, J., Robertson, S., Kennedy, M., Wall, C. and Keller, G.** (1999). Development of erythroid and
914 myeloid progenitors in the yolk sac and embryo proper of the mouse. *Development* **126**, 5073–5084.

915 **Pongratz, I., Antonsson, C., Whitelaw, M. L. and Poellinger, L.** (1998). Role of the PAS domain in
916 regulation of dimerization and DNA binding specificity of the dioxin receptor. *Mol. Cell. Biol.* **18**,
917 4079–4088.

918 **Prasch, A. L., Tanguay, R. L., Mehta, V., Heideman, W. and Peterson, R. E.** (2006). Identification of
919 zebrafish ARNT1 homologs: 2,3,7,8-tetrachlorodibenzo-p-dioxin toxicity in the developing zebrafish
920 requires ARNT1. *Mol. Pharmacol.* **69**, 776–787.

921 **Qian, F., Zhen, F., Ong, C., Jin, S.-W., Meng Soo, H., Stainier, D. Y. R., Lin, S., Peng, J. and Wen,**
922 **Z.** (2005). Microarray analysis of zebrafish cloche mutant using amplified cDNA and identification of
923 potential downstream target genes. *Dev. Dyn.* **233**, 1163–1172.

924 **Ramírez-Bergeron, D. L., Runge, A., Dahl, K. D. C., Fehling, H. J., Keller, G. and Simon, M. C.**
925 (2004). Hypoxia affects mesoderm and enhances hemangioblast specification during early
926 development. *Development* **131**, 4623–4634.

927 **Reischauer, S., Stone, O. A., Villasenor, A., Chi, N., Jin, S.-W., Martin, M., Lee, M. T., Fukuda, N.,**
928 **Marass, M., Witty, A., et al.** (2016). Cloche is a bHLH-PAS transcription factor that drives haemato-
929 vascular specification. *Nature* **535**, 294–298.

930 **Sekine, H., Mimura, J., Yamamoto, M. and Fujii-Kuriyama, Y.** (2006). Unique and overlapping
931 transcriptional roles of arylhydrocarbon receptor nuclear translocator (Arnt) and Arnt2 in xenobiotic
932 and hypoxic responses. *J. Biol. Chem.* **281**, 37507–37516.

933 **Shalaby, F., Ho, J., Stanford, W. L., Fischer, K. D., Schuh, A. C., Schwartz, L., Bernstein, A. and**
934 **Rossant, J.** (1997). A requirement for Flk1 in primitive and definitive hematopoiesis and
935 vasculogenesis. *Cell* **89**, 981–990.

936 **Souder, J. P. and Gorelick, D. A.** (2019). ahr2, But Not ahr1a or ahr1b, Is Required for Craniofacial
937 and Fin Development and TCDD-dependent Cardiotoxicity in Zebrafish. *Toxicol. Sci.* **170**, 25–44.

938 **Stainier, D. Y., Lee, R. K. and Fishman, M. C.** (1993). Cardiovascular development in the zebrafish. I.
939 Myocardial fate map and heart tube formation. *Development* **119**, 31–40.

940 **Stainier, D. Y., Weinstein, B. M., Detrich, H. W., Zon, L. I. and Fishman, M. C.** (1995). Cloche, an
941 early acting zebrafish gene, is required by both the endothelial and hematopoietic lineages.
942 *Development* **121**, 3141–3150.

943 **Sumanas, S. and Lin, S.** (2006). Ets1-related protein is a key regulator of vasculogenesis in zebrafish.
944 *PLoS Biol.* **4**, e10.

945 **Sumanas, S., Jorniak, T. and Lin, S.** (2005). Identification of novel vascular endothelial-specific genes
946 by the microarray analysis of the zebrafish cloche mutants. *Blood* **106**, 534–541.

947 **Tanguay, R. L., Andreasen, E., Heideman, W. and Peterson, R. E.** (2000). Identification and
948 expression of alternatively spliced aryl hydrocarbon nuclear translocator 2 (ARNT2) cDNAs from
949 zebrafish with distinct functions. *Biochim. Biophys. Acta* **1494**, 117–128.

950 **Thompson, M. A., Ransom, D. G., Pratt, S. J., MacLennan, H., Kieran, M. W., Detrich, H. W., Vail,**
951 **B., Huber, T. L., Paw, B., Brownlie, A. J., et al.** (1998). The cloche and spadetail genes
952 differentially affect hematopoiesis and vasculogenesis. *Dev. Biol.* **197**, 248–269.

953 **Vogeli, K. M., Jin, S.-W., Martin, G. R. and Stainier, D. Y. R.** (2006). A common progenitor for
954 haematopoietic and endothelial lineages in the zebrafish gastrula. *Nature* **443**, 337–339.

955 **Wang, Q., Stacy, T., Binder, M., Marin-Padilla, M., Sharpe, A. H. and Speck, N. A.** (1996).
956 Disruption of the Cbfa2 gene causes necrosis and hemorrhaging in the central nervous system and
957 blocks definitive hematopoiesis. *Proc Natl Acad Sci USA* **93**, 3444–3449.

958 **Westerfield, M.** (2000). *The Zebrafish Book. A Guide for the Laboratory Use of Zebrafish (Danio*
959 *Rerio).* 4th ed. Eugene, OR: University of Oregon Press.

960 **Wu, D. and Rastinejad, F.** (2017). Structural characterization of mammalian bHLH-PAS transcription
961 factors. *Curr. Opin. Struct. Biol.* **43**, 1–9.

Figure 1

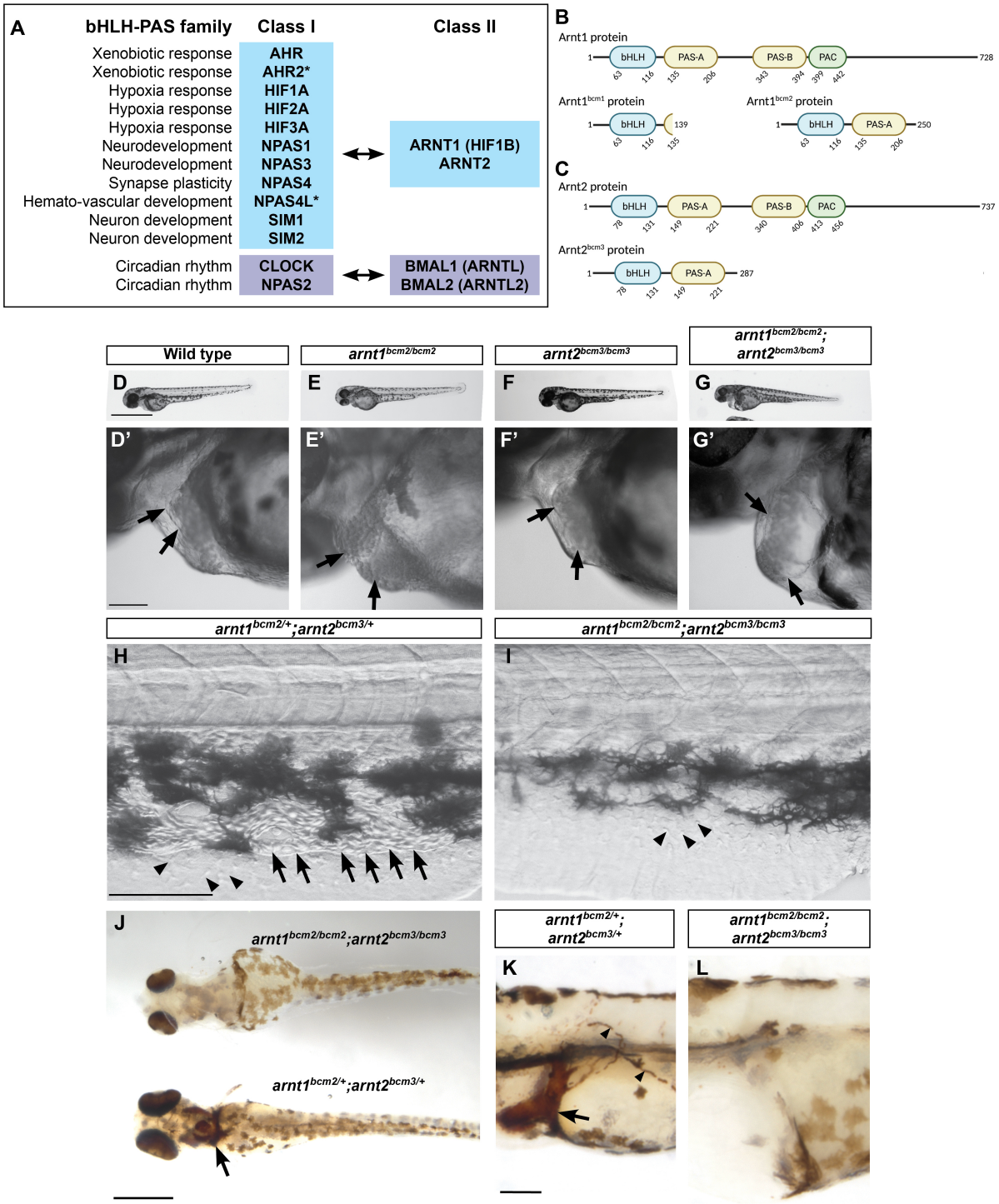
A
bHLH-PAS family
Class I
Class II
Xenobiotic response
Xenobiotic response
Hypoxia response
Hypoxia response
Hypoxia response
Neurodevelopment
Neurodevelopment
Synapse plasticity
Hemato-vascular development
Neuron development
Neuron development
AHR
AHR2*
HIF1A
HIF2A
HIF3A
NPAS1
NPAS3
NPAS4
NPAS4L*
SIM1
SIM2
ARNT1 (HIF1B)
ARNT2
Circadian rhythm
Circadian rhythm
CLOCK
NPAS2
BMAL1 (ARNTL)
BMAL2 (ARNTL2)
B
Arnt1 protein
bHLH
PAS-A
PAS-B
PAC
Arnt1bcm1 protein
Arnt1bcm2 protein
C
Arnt2 protein
Arnt2bcm3 protein
Wild type
arnt1bcm2/bcm2
arnt2bcm3/bcm3
arnt1bcm2/bcm2; arnt2bcm3/bcm3
arnt1bcm2/+;arnt2bcm3/+
arnt1bcm2/bcm2;arnt2bcm3/bcm3
arnt1bcm2/bcm2;arnt2bcm3/bcm3
arnt1bcm2/+;arnt2bcm3/+
arnt1bcm2/+; arnt2bcm3/+
arnt1bcm2/bcm2; arnt2bcm3/bcm3

Figure 2

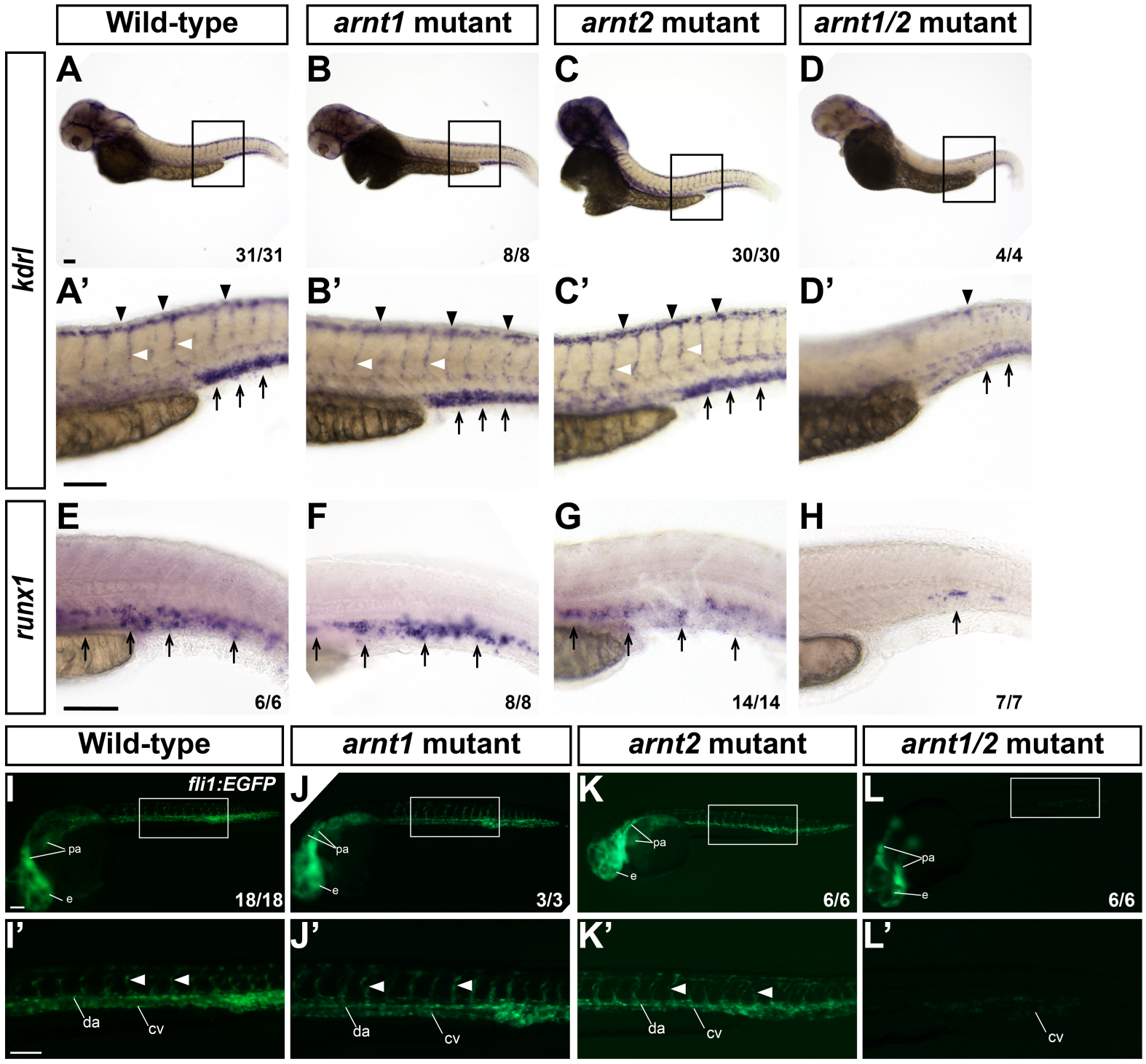
Wild-type
arnt1 mutant
arnt2 mutant
arnt1/2 mutant
kdrl
runx1
A
B
C
D
A'
B'
C'
D'
E
F
G
H
31/31
8/8
30/30
4/4
6/6
8/8
14/14
7/7
Wild-type
arnt1 mutant
arnt2 mutant
arnt1/2 mutant
fli1:EGFP
I
J
K
L
I'
J'
K'
L'
pa
e
da
cv
18/18
3/3
6/6
6/6

Figure 3

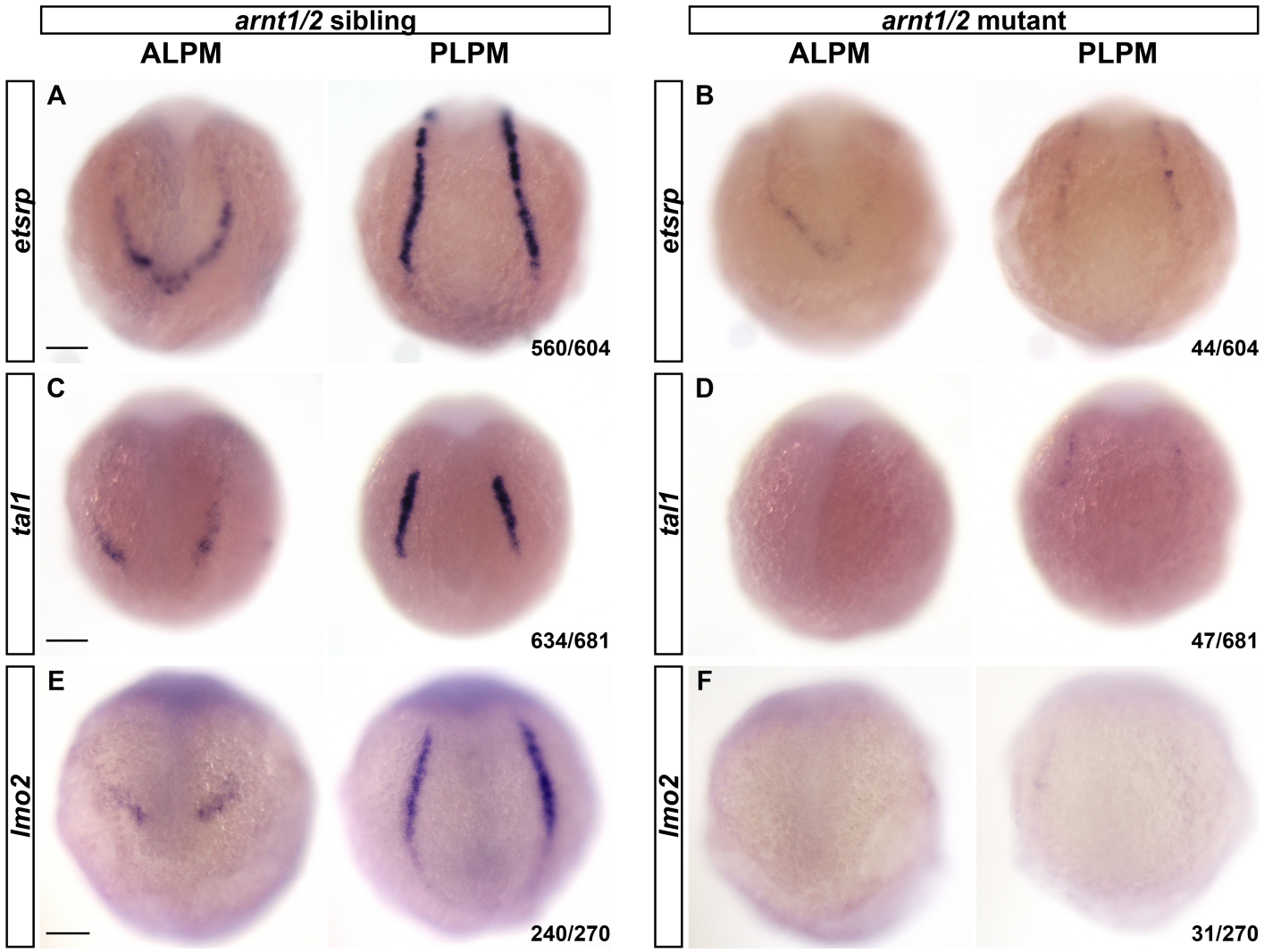
arnt1/2 sibling
arnt1/2 mutant
ALPM
PLPM
ALPM
PLPM
etsrp
tal1
lmo2
A
B
C
D
E
F
560/604
44/604
634/681
47/681
240/270
31/270

Figure 4

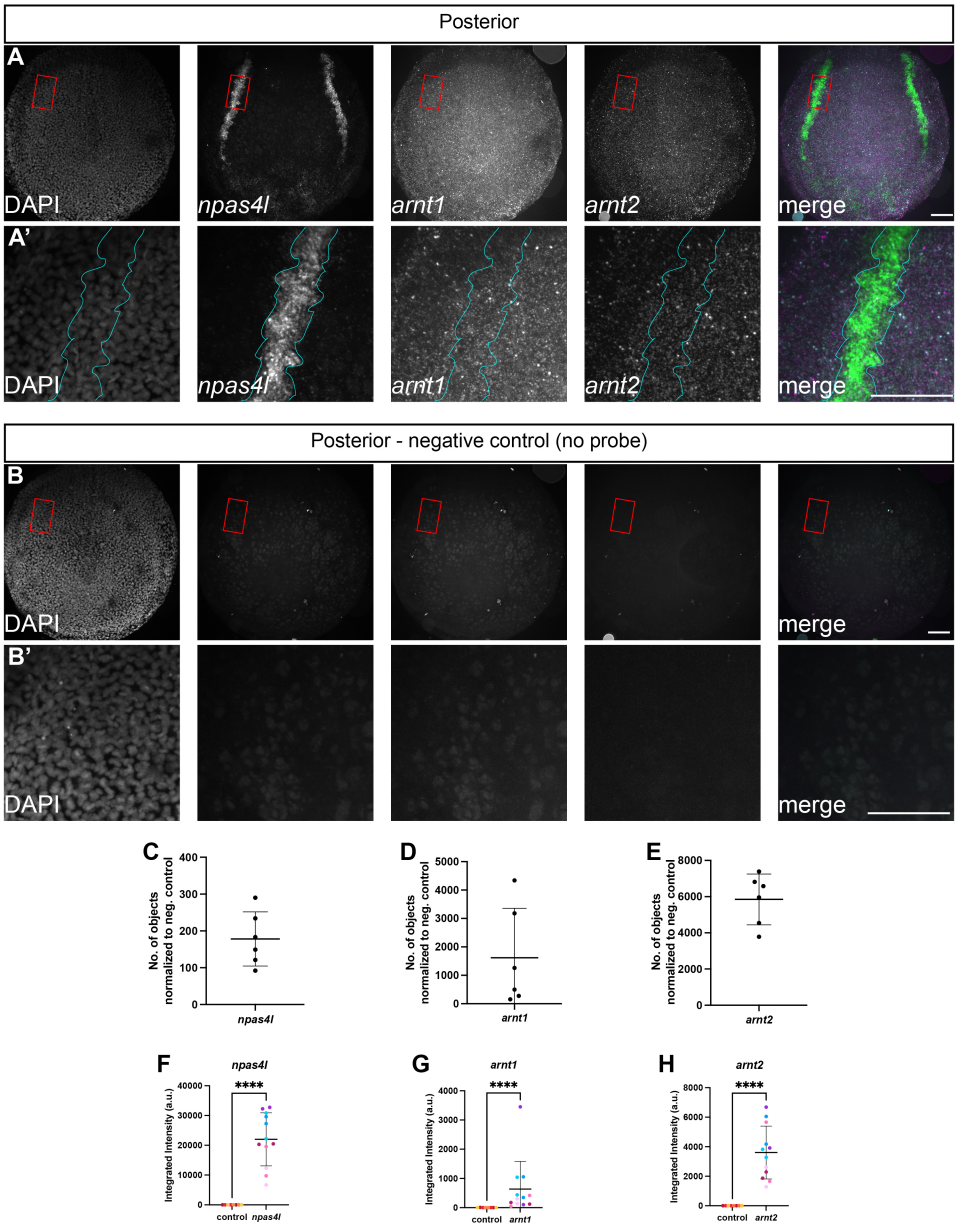
Posterior
A
DAPI
npas4l
arnt1
arnt2
merge
A'
DAPI
npas4l
arnt1
arnt2
merge
Posterior - negative control (no probe)
B
DAPI
merge
B'
DAPI
merge
C
No. of objects normalized to neg. control
400
300
200
100
0
npas4l
D
No. of objects normalized to neg. control
5000
4000
3000
2000
1000
0
arnt1
E
No. of objects normalized to neg. control
8000
6000
4000
2000
0
arnt2
F
npas4l
Integrated Intensity (a.u.)
40000
30000
20000
10000
0
****
control
npas4l
G
arnt1
Integrated Intensity (a.u.)
4000
3000
2000
1000
0
****
control
arnt1
H
arnt2
Integrated Intensity (a.u.)
8000
6000
4000
2000
0
****
control
arnt2

Figure 5

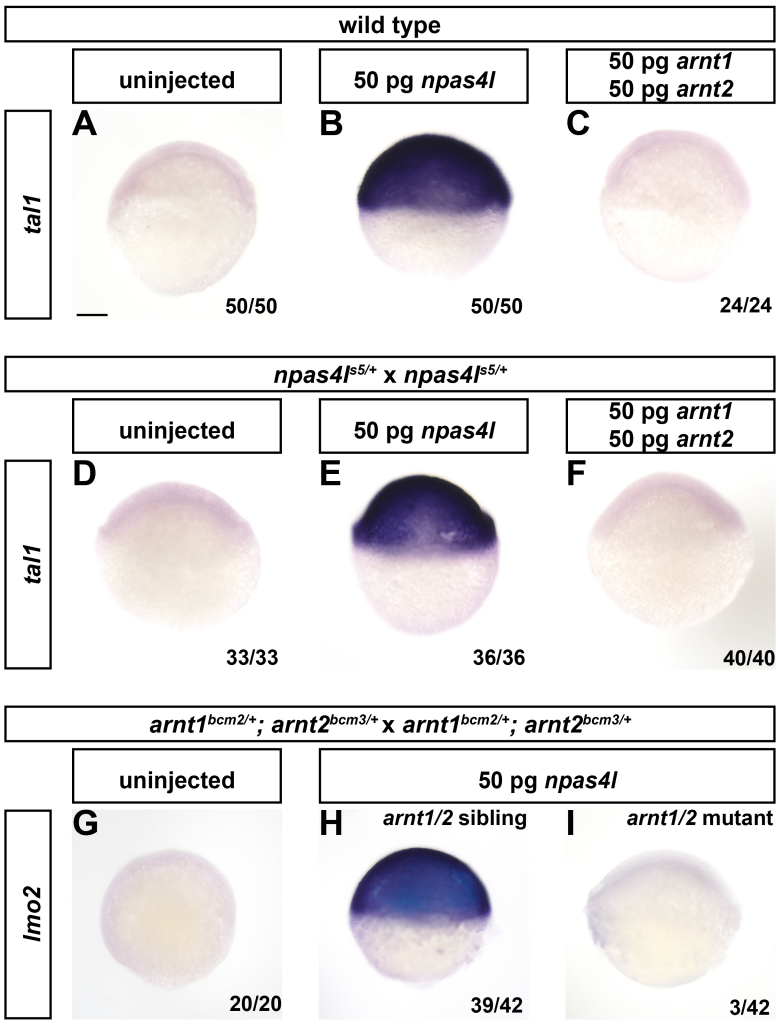
wild type
uninjected
50 pg npas4l
50 pg arnt1
50 pg arnt2
tal1
A
B
C
50/50
50/50
24/24
npas4l s5/+ x npas4l s5/+
uninjected
50 pg npas4l
50 pg arnt1
50 pg arnt2
tal1
D
E
F
33/33
36/36
40/40
arnt1 bcm2/+; arnt2 bcm3/+ x arnt1 bcm2/+; arnt2 bcm3/+
uninjected
50 pg npas4l
lmo2
G
H
arnt1/2 sibling
I
arnt1/2 mutant
20/20
39/42
3/42

Figure 6

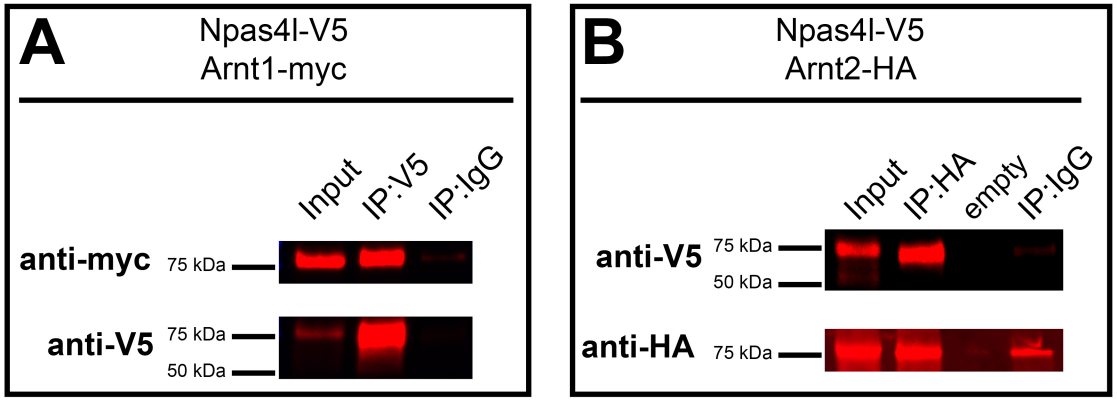
A
Npas4l-V5
Arnt1-myc
Input
IP:V5
IP:IgG
anti-myc
75 kDa
anti-V5
75 kDa
50 kDa
B
Npas4l-V5
Arnt2-HA
Input
IP:HA
empty
IP:IgG
anti-V5
75 kDa
50 kDa
anti-HA
75 kDa

Figure 7

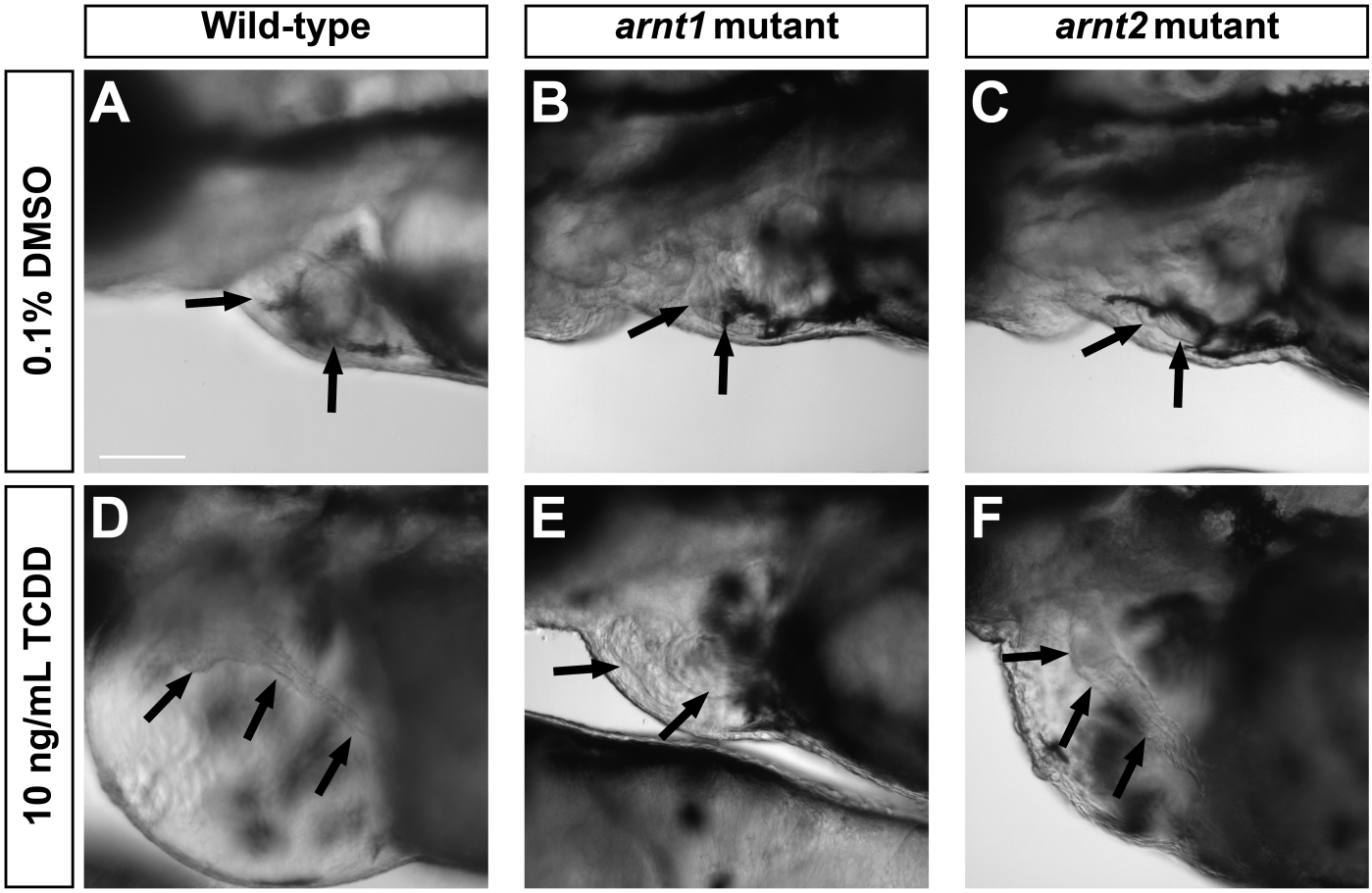
Wild-type
arnt1 mutant
arnt2 mutant
0.1% DMSO
10 ng/mL TCDD
A
B
C
D
E
F

Supplemental files

Supplemental Table 1. Oligonucleotide primers and probes used in this study

Supplemental Table 2. Genotype versus phenotype correlation of embryos probed for *etsrp* (related to Figure 3)

Supplemental Table 3. Genotype versus phenotype correlation of embryos probed for *tal1* (related to Figure 3)

Supplemental Table 4. Genotype versus phenotype correlation of embryos probed for *lmo2* (related to Figure 3)

Supplemental Table 5. Genotype versus phenotype correlation of embryos probed for *egfl7* (related to Supplemental Figure 1)

Supplemental Table 6. Genotype versus phenotype correlation of embryos probed for *npas4l* (related to Supplemental Figure 2)

Supplemental Figure 1. *arnt1/2* mutants show reduced expression of *egfl7* in the lateral plate mesoderm (related to Figure 3)

Supplemental Figure 2. *arnt1/2* mutants and *arnt1/2* siblings have normal expression of *npas4l* (related to Figure 3)

Supplemental Figure 3. *npas4l* and *arnt2* mRNA, but not *arnt1*, are enriched in the posterior lateral plate mesoderm (related to Figure 4)

Supplemental Figure 4. *arnt1* mutants, but not *arnt2* mutants, are resistant to TCDD toxicity (related to Figure 7)

Movie 1.mp4 *arnt1*$^{bcm2/+}$;*arnt2*$^{bcm3/+}$ 50 hpf, head and heart
Movie 2.mp4 *arnt1*$^{bcm2/+}$;*arnt2*$^{bcm3/+}$ 50 hpf, blood flow in tail
Movie 3.mp4 *arnt1*$^{bcm2/bcm2}$;*arnt2*$^{bcm3/bcm3}$ 50 hpf, head and heart
Movie 4.mp4 *arnt1*$^{bcm2/bcm2}$;*arnt2*$^{bcm3/bcm3}$ 50 hpf, blood flow in tail
Movie 5.mp4 *arnt1*$^{bcm2/+}$;*arnt2*$^{bcm3/+}$ 2 dpf, head and heart
Movie 6.mp4 *arnt1*$^{bcm2/+}$;*arnt2*$^{bcm3/+}$ 2 dpf, blood flow in tail
Movie 7.mp4 *arnt1*$^{bcm2/bcm2}$;*arnt2*$^{bcm3/bcm3}$ 2 dpf, head and heart
Movie 8.mp4 *arnt1*$^{bcm2/bcm2}$;*arnt2*$^{bcm3/bcm3}$ 2 dpf, blood flow in tail

Movies 1 and 2 from the same embryo, movies 3 and 4 from the same embryo, movies 5 and 6 from the same embryo, movies 7 and 8 from the same embryo.

Primer	Forward 5'-3'	Reverse 5'-3'	Reference
bcm1-gRNA	TAGGATGGTTTATAGGTGCCAT	AAACATGGCACCTATAAACCAT	
bcm1-HRMA	ATGGCCGTATCACACATGAAG	AGACCTGGTCTGTGAGAAAGGAT	
bcm1-seq	AAATGACCGCCTACATCA	TGCCTACAGTGCATTGTT	
bcm2-gRNA	TAGGCGACTGTGAGGATGAGTA	AAACTACTCATCCTCACAGTCG	
bcm2-HRMA	GTGAAGAAGGAGGGTGGTCA	CATTCTGCAGATGAAGGAGCG	
bcm2-ISHseq	GCAAATATATCTTAAGGGGGCCAAT	TCCAGGTCAGTGTCTTCACCA	
bcm2-ISHseq	TCAGACATACTGTGAAACATTTCTTGC	CACCATGAAATAGGAGCAGCTTG	
bcm2-seq	AAACTCACTATCCTGCGCATG	AGACCTGGTCTGTGAGAAAGGAT	
bcm3-gRNA	TAGGTCTCGGTCCGTCTAAGGA	AAACTCCTTAGACGGACCGAGA	
bcm3-HRMA	TGTGAGCCGAATGTTGGCT	ACAACAGAGTACTGCGCTTCA	
bcm3-ISHseq	CCAGGTAAAAACATGACCTGTTCC	CATTGAAACAATATGCAGCAATGA	
bcm3-ISHseq	TGTCTACAAAATCCTCCACACTGCT	TTGAATATTTCAAAATCACATGCAG	
bcm3-seq	ACATGACCTGTTCCATACC	TCAGTGCTTCAGTGTCTT	
egfl7- probe	GCGCGGTGCTCTTCATCAG	AGCCTCCTTACACTCGTCCACATC	
lmo2 -probe	GTGCGGCAGATGGTCTTTCGGAACC	CTGCAACCCAACACTGGGAAACCTG	(Sun *et al*. 2018)

Table S1. Oligonucleotide primers and probes used in this study

Genotype		Phenotype (number of embryos)	
Allele designation	Number of mutant alleles	Normal expression	Reduced expression
arnt1 $^{bcm2/bcm2}$; *arnt2* $^{bcm3/bcm3}$	4	2	24
arnt1 $^{bcm2/bcm2}$; *arnt2* $^{bcm3/+}$	3	4	0
arnt1 $^{bcm2/+}$; *arnt2* $^{bcm3/bcm3}$		4	0
arnt1 $^{bcm2/+;}$ *arnt2* $^{bcm3/+}$	2	5	0
arnt1 $^{bcm2/bcm2}$		3	0
arnt2 $^{bcm3/bcm3}$		2	0
arnt1 $^{bcm2/+}$	1	4	0
arnt2 $^{bcm3/+}$		3	0
wild-type	0	1	0

Table S2. Genotype versus phenotype correlation of embryos probed for *etsrp* (See Figure 3). There was a significant correlation between the number of mutant alleles and *etsrp* expression phenotype, $r(47)=-0.9$, $p<0.001$

Genotype		Phenotype (number of embryos)	
Allele designation	Number of mutant alleles	Normal expression	Reduced expression
arnt1 $^{bcm2/bcm2}$; *arnt2* $^{bcm3/bcm3}$	4	1	14
arnt1 $^{bcm2/bcm2}$; *arnt2* $^{bcm3/+}$	3	3	3
arnt1 $^{bcm2/+}$; *arnt2* $^{bcm3/bcm3}$		1	0
arnt1 $^{bcm2/+;}$ *arnt2* $^{bcm3/+}$	2	1	0
arnt1 $^{bcm2/bcm2}$		0	0
arnt2 $^{bcm3/bcm3}$		0	0
arnt1 $^{bcm2/+}$	1	1	0
arnt2 $^{bcm3/+}$		2	0
wild-type	0	0	0

Table S3. Genotype versus phenotype correlation of embryos probed for *tal1* (See Figure 3). There was a significant correlation between the number of mutant alleles and *tal1* expression phenotype, $r(25)=-0.6$, $p<0.001$

Genotype		Phenotype (number of embryos)	
Allele designation	Number of mutant alleles	Normal expression	Reduced expression
arnt1 $^{bcm2/bcm2}$; *arnt2* $^{bcm3/bcm3}$	4	5	7
arnt1 $^{bcm2/bcm2}$; *arnt2* $^{bcm3/+}$	3	23	5
arnt1 $^{bcm2/+}$; *arnt2* $^{bcm3/bcm3}$		13	3
arnt1 $^{bcm2/+;}$ *arnt2* $^{bcm3/+}$	2	47	3
arnt1 $^{bcm2/bcm2}$		5	0
arnt2 $^{bcm3/bcm3}$		10	2
arnt1 $^{bcm2/+}$	1	28	1
arnt2 $^{bcm3/+}$		19	2
wild-type	0	7	2

Table S4. Genotype versus phenotype correlation of embryos probed for *lmo2* (See Figure 3). There was a significant correlation between the number of mutant alleles and *lmo2* expression phenotype, $r(184)=-0.2$, $p<0.005$

Genotype		Phenotype (number of embryos)	
Allele designation	Number of mutant alleles	Normal expression	Reduced expression
arnt1 $^{bcm2/bcm2}$; *arnt2* $^{bcm3/bcm3}$	4	2	6
arnt1 $^{bcm2/bcm2}$; *arnt2* $^{bcm3/+}$	3	4	0
arnt1 $^{bcm2/+}$; *arnt2* $^{bcm3/bcm3}$		6	1
arnt1 $^{bcm2/+;}$ *arnt2* $^{bcm3/+}$	2	6	1
arnt1 $^{bcm2/bcm2}$		13	2
arnt2 $^{bcm3/bcm3}$		2	0
arnt1 $^{bcm2/+}$	1	36	0
arnt2 $^{bcm3/+}$		3	0
wild-type	0	12	0

Table S5. Genotype versus phenotype correlation of embryos probed for *egfl7* (See Supplemental Figure 1). There was a significant correlation between the number of mutant alleles and *egfl7* expression phenotype, $r(94)=-0.5, p<0.001$

Genotype		Phenotype (number of embryos)	
Allele designation	Number of mutant alleles	Normal expression	Reduced expression
arnt1 $^{bcm2/bcm2}$; *arnt2* $^{bcm3/bcm3}$	4	2	0
arnt1 $^{bcm2/bcm2}$; *arnt2* $^{bcm3/+}$	3	4	0
arnt1 $^{bcm2/+}$; *arnt2* $^{bcm3/bcm3}$		11	0
arnt1 $^{bcm2/+;}$ *arnt2* $^{bcm3/+}$	2	19	1
arnt1 $^{bcm2/bcm2}$		3	1
arnt2 $^{bcm3/bcm3}$		5	0
arnt1 $^{bcm2/+}$	1	11	0
arnt2 $^{bcm3/+}$		5	0
wild-type	0	8	0

Table S6. Genotype versus phenotype correlation of embryos probed for *npas4l* (See Supplemental Figure 2). There was no significant correlation between the number of mutant alleles and *npas4l* expression phenotype, $r(69)=-0.05,\ p>0.05$

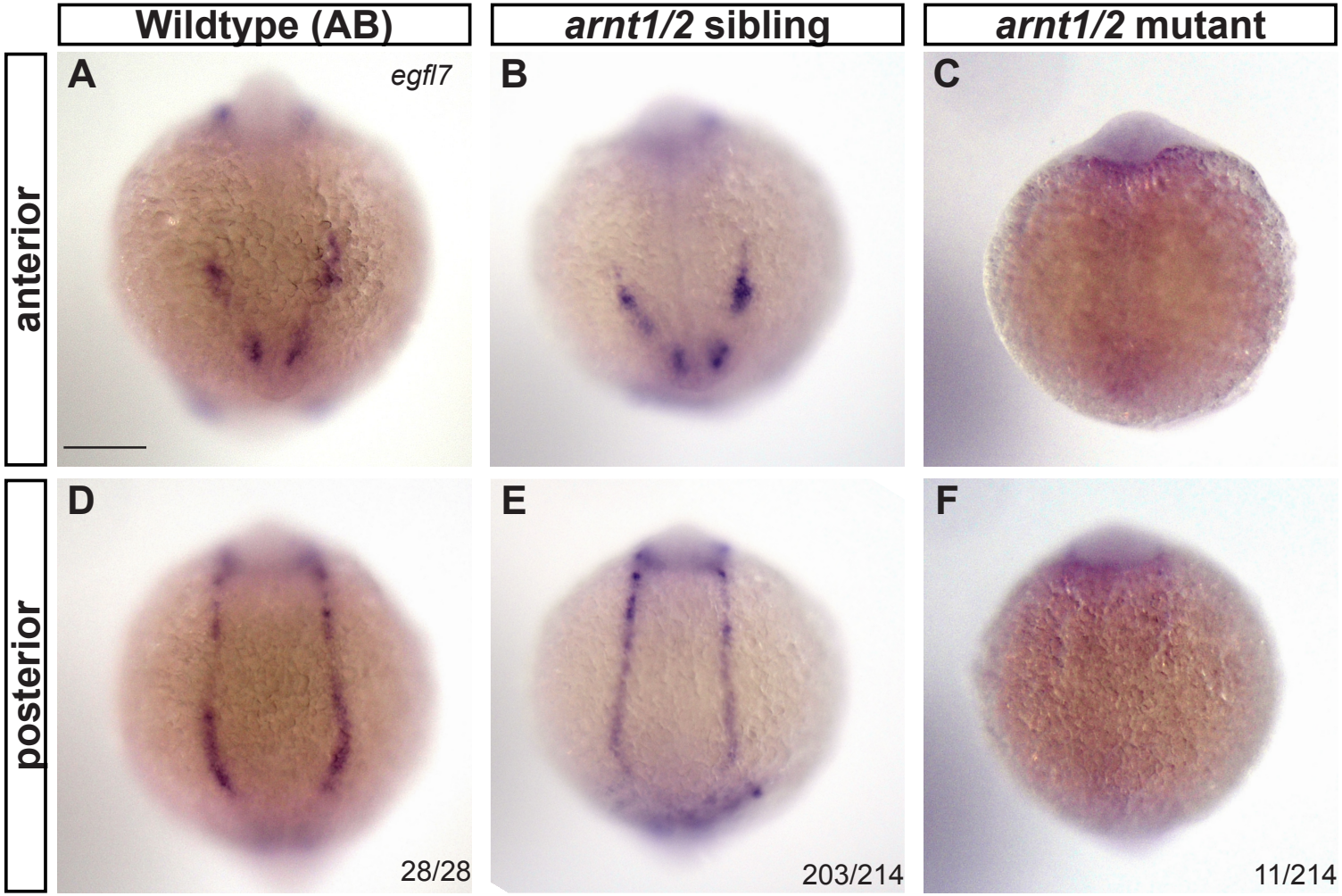

Supplemental Figure 1. *arnt1/2* mutants show reduced expression of *egfl7* in the lateral plate mesoderm. Whole-mount in situ hybridization for *egfl7* was performed on 10 somite stage embryos from *arnt1*$^{bcm2/+}$;*arnt2*$^{bcm3/+}$ parents (N=2 biological replicates, 94-120 embryos per clutch, 214 total embryos) or from wildtype (AB) parents (N=1 biological replicate, 28 total embryos). (**A** and **D**) expression of *egfl7* in wildtype embryos is restricted to the anterior lateral plate mesoderm (ALPM) (**A**) and the posterior lateral plate mesoderm (PLPM) (**D**). (**B** and **E**) Expression of *egfl7* was observed in the ALPM (**B**) and the PLPM (**E**) in 95% of embryos from *arnt1*$^{bcm2/+}$; *arnt2*$^{bcm3/+}$ parents (n=203 out of 214 total embryos). (**C** and **F**) Limited or no expression of *egfl7* was observed in the ALPM and PLPM in 5% of embryos from *arnt1*$^{bcm2/+}$;*arnt2*$^{bcm3/+}$ parents (n=11 out of 214 total embryos), which is consistent with the expected Mendelian ratio of 6.25% *arnt1*$^{bcm2/bcm2}$;*arnt2*$^{bcm3/bcm3}$ (*arnt1/2* mutants, binomial test, $p<0.05$). All embryos are oriented with dorsal towards the top of the image. Fractions in bottom right corners refer to the number of embryos with the indicated phenotype over the total number of embryos examined. See **Supplemental Table 5** for genotype frequencies. Scale bar, 100µm.

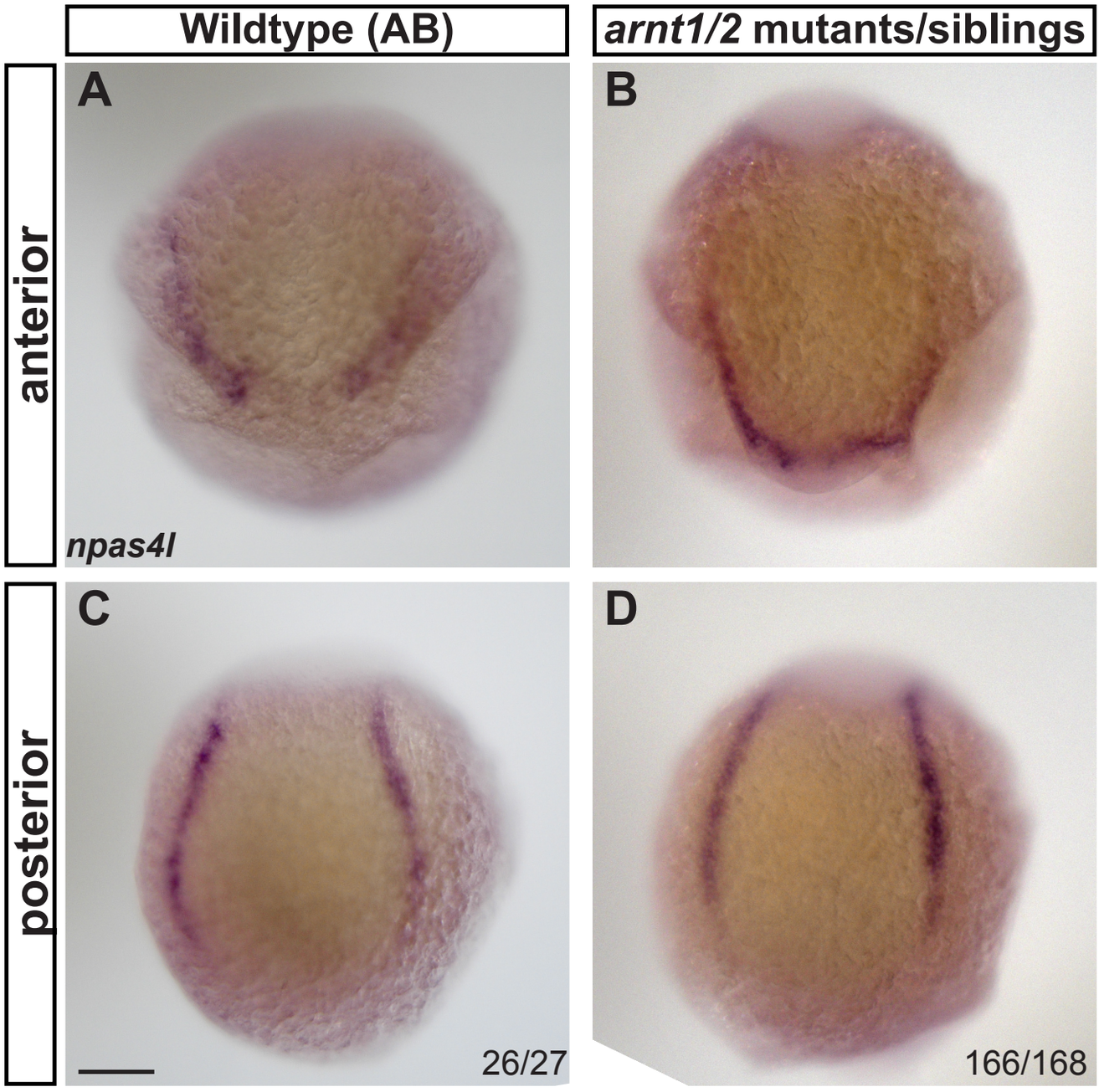

Supplemental Figure 2. *arnt1/2* mutants and *arnt1/2* siblings have normal expression of *npas4l*. Whole-mount in situ hybridization for *npas4l* on 4 somite stage embryos from *arnt1*$^{bcm2/+}$; *arnt2*$^{bcm3/+}$ parents (N=2 biolgical replicates, 68-100 embryos per clutch, n= 168 embryos total) or from wild-type (AB) parents (N=1 biological replicate, n=27 embryos total). (**A**) Expression of *npas4l* was observed in the anterior lateral plate mesoderm (ALPM) of wild-type embryos. (**B**) Expression of *npas4l* was observed in the ALPM embryos from *arnt1*$^{bcm2/+}$; *arnt2*$^{bcm3/+}$ parents, including the *arnt1/2* mutants. (**C**) Expression of *npas4l* was observed in the PLPM of wild-type embryos. (**D**) Expression of *npas4l* was observed in the posterior lateral plate meosderm (PLPM) embryos from *arnt1*$^{bcm2/+}$; *arnt2*$^{bcm3/+}$ parents, including the *arnt1/2* mutants. Embryos oriented with dorsal towards the top of the image. The fractions in the right-hand corners of **C** and **D** refer to the number of embryos with the represented phenotypes over the total number of embryos. Scale bar, 100 µm.

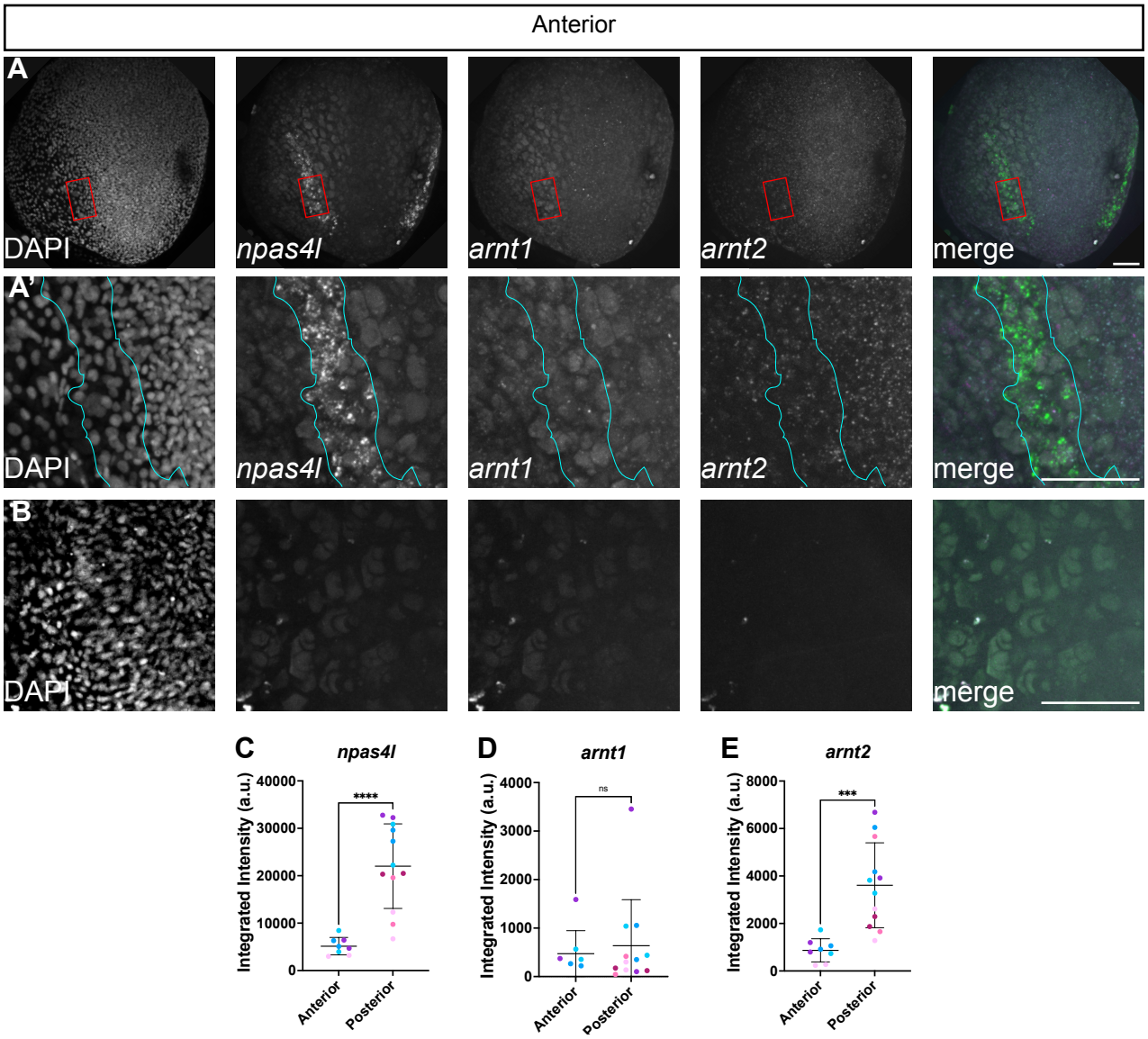

Supplemental Figure 3. Expression of *npas4l*, *arnt1* and *arnt2* mRNA in the anterior lateral plate mesoderm. Companion to Figure 4, which shows expression in the posterior lateral plate mesoderm. Whole-mount *in situ* hybridization chain reaction was performed on wild-type (AB) embryos at the 4 somite stage. **(A)** Embryos were probed for *npas4l, arnt1,* and *arnt2* expression and counter-stained with DAPI. **(A')** Higher magnification views of the boxed areas in (A) shows the anterior lateral plate mesoderm, outlined in cyan. N=3 biological replicates, 5-9 embryos per replicate, 22 embryos total. **(B)** To demonstrate that the observed labeling is not autofluorescence of the embryo or the yolk, wild-type embryos were processed identically to those in (A), but no anti-sense RNA probe sets were added. The views in (B) are identical magnification as those in (A'). N=3 biological replicates, 6-12 embryos per replicate, 28 embryos total. Images are maximum intensity projections from z-stacks taken every 2.5 µm. In merged panels, *npas4l* is green, *arnt1* is magenta, *arnt2* is cyan. The anterior portion of the embryo is in view, dorsal is towards the top of the image. Scale bars = 100 µm. **(C-E)** *npas4l* and *arnt2* mRNA, but not *arnt1*, are enriched in the posterior lateral plate mesoderm. Quantification of the fluorescence integrated intensity of *npas4l, arnt1,* and *arnt2* labeling within the *npas4l*-positive cells of the anterior and posterior lateral plate mesoderm (see panel A and Figure 4). We calculated the integrated intensity of fluorescence (pixel area, pixel intensity) over each side of the anterior or posterior LPM in maximum intensity projections. Each point represents the integrated intensity from one side of the LPM from a single embryo (right or left side), where each embryo has two bilateral *npas4l*-positive regions of the LPM. Points of the same color are measurements from opposite sides of the LPM from the same embryo. 6 representative embryos were used for this analysis, in 2 of these embryos the anterior LPM was damaged during imaging and could not be analyzed. **(C)** *npas4l* expression was statistically significantly increased in the posterior versus anterior LPM, Welch's t-test, $t(12.36)=6.4$, $p<0.0001$. **(D)** *arnt1* was expressed at similar levels in the anterior and posterior, Mann-Whitney, $U=45$, $p>0.05$. **(E)** *arnt2* expression was statistically significantly increased in the posterior versus anterior LPM, Welch's t-test, $t(11)= 5.0$, $p<0.0005$.

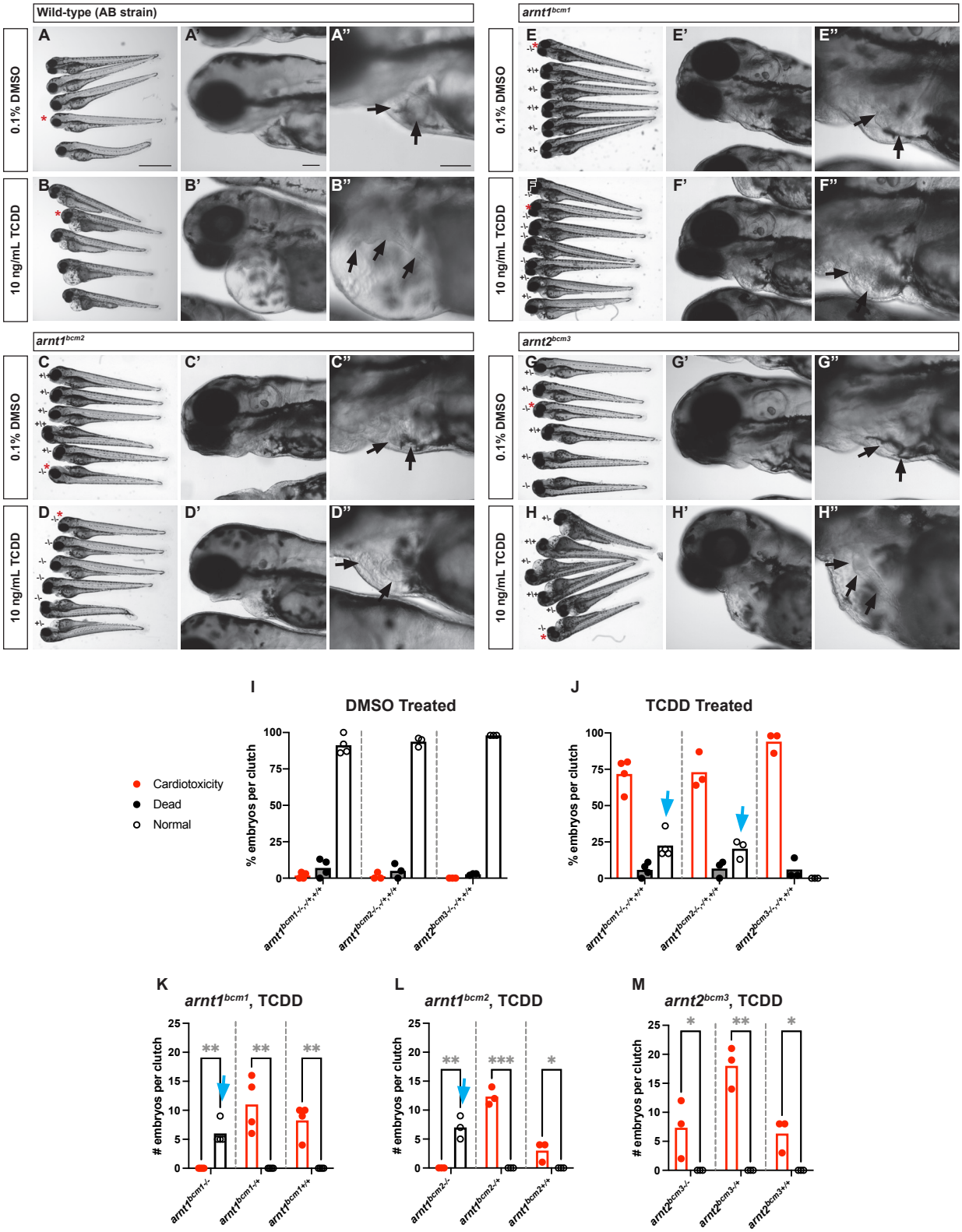

Supplemental Figure 4. *arnt1* mutants, but not *arnt2* mutants, are resistant to TCDD toxicity. Representative images of larvae at 3 days post fertilization (dpf) exposed to either DMSO or TCDD. Mutant larvae were derived from heterozygous parents and genotyped following imaging (denoted as wild-type +/+, heterozygous -/+, or homozygous -/- in panels **C-H**). (**A-H**) overview images of treated larvae, red asterisks denote larvae detailed in panels A'-H' and A"-H". Black arrows in panels A"-H" point to the heart within the pericardial cavity. Pericardial edema and incomplete heart looping is present in 100% of wild-type (n=3 biological replicates per genotype, 10-60 larvae per clutch per treatment, 157 larvae total) and *arnt2* mutant larvae (n=3 biological replicates per genotype, 40-50 larvae per clutch per treatment, 253 larvae total). In contrast, 100% of *arnt1* mutants (3-4 clutches per allele, 21-36 larvae per clutch per treatment, 533 larvae total, 248 larvae from allele bcm1 and 285 larvae allele from bcm2) are resistant to TCDD cardiotoxicity. Scale bars, 100 µm. (**I** and **J**) Percent larvae from each clutch demonstrating cardiotoxicity (red dots/red bars), mortality (black dots/gray bars), or normal development (white dots/white bars) at 3 dpf. All clutches were derived from heterozygous parents and embryos were analyzed prior to genotyping. Each clutch contain a mix of wild-type, heterozygous, and homozygous larvae. Each dot represents the percent of larvae from a single clutch and bars represent the mean. (**J**) In clutches derived from *arnt2*$^{bcm3/+}$ parents, nearly 100% of embryos exhibited cardiotoxicity following TCDD exposure. In clutches derived from *arnt1* heterozygous parents, approximately 75% of embryos exhibited cardiotoxicity or death, while 25% of embryos exhibited a normal phenotype (blue arrows), consistent with the expected Mendelian ratio of *arnt1* homozygotes. Normal larvae were not observed in wild-type or *arnt2* mixed clutches exposed to TCDD. (**K-M**) We genotyped the embryos from (**J**) and graphed the number of embryos per clutch exhibiting cardiotoxicity (red dots/red bars) or normal development (white dots/white bars). Each dot represents the number of larvae from a single clutch. (**K,L**) All *arnt1* homozygous mutants (*bcm1* or *bcm2*) exhibited normal phenotype following TCDD exposure (blue arrows), while *arnt1* heterozygotes and (**M**) *arnt2* mutants exhibited cardiotoxicity. Unpaired Welch's t-tests, * $p<0.05$, ** $p<0.005$, and *** $p<0.001$.